Reliable Slicing of 5G Transport Networks with Bandwidth Squeezing and Multi-path Provisioning

Nashid Shahriar, *Student Member, IEEE*, Sepehr Taeb, Shihabur Rahman Chowdhury, *Student Member, IEEE*, Mubeen Zulfiqar, Massimo Tornatore, *Senior Member, IEEE*, Raouf Boutaba, *Fellow, IEEE*, Jeebak Mitra, and Mahdi Hemmati *Member, IEEE*

***Abstract*—5G network slicing allows partitioning of network resources to meet stringent end-to-end service requirements across multiple network segments, from access to transport. These requirements are shaping technical evolution in each of these segments. In particular, the transport segment is currently evolving in the direction of elastic optical networks (EONs), a new generation of optical networks supporting a flexible optical-spectrum grid and novel elastic transponder capabilities. In this paper, we focus on the reliability of 5G transport-network slices in EON. Specifically, we consider the problem of slicing 5G transport networks, *i.e.*, establishing virtual networks on 5G transport, while providing dedicated protection. As dedicated protection requires a large amount of backup resources, our proposed solution incorporates two techniques to reduce backup resources: (i) bandwidth squeezing, *i.e.*, providing a reduced protection bandwidth than the original request; and (ii) survivable multi-path provisioning. We leverage the capability of EONs to fine tune spectrum allocation and adapt modulation format and forward error correction for allocating spectrum resources. Our numerical evaluation over realistic network topologies quantifies the spectrum savings achieved by employing EON over traditional fixed-grid optical networks, and provides new insights on the impact of bandwidth squeezing and multi-path provisioning on spectrum utilization. One key takeaway from our evaluation is that multi-path provisioning can guarantee up to 40% of the bandwidth requested by a VN during failures by provisioning only 10% additional spectrum resources. This also caused VN blocking ratio for BSR up to 40% to remain very close to that of the no-backup case.**

***Index Terms*—5G slicing, transport network, elastic optical network, fault Management, optical networks, virtual networks.**

I. Introduction

Transport networks employing the latest advances in elastic optical networking will form the backbone of the fifth-generation (5G) networks and beyond [2]–[4]. Transport-network capacity must be easily partitionable to facilitate network slicing for 5G services such as enhanced mobile broadband and ultra-reliable low latency communications [5]. Elastic Optical Networks (EONs) are an excellent choice for establishing transport network slices, thanks to their ability to tailor network resources based on service requirements [6].

Network slices are usually provided in the form of virtual networks (VNs) (*i.e.*, collection of virtual nodes and virtual links (VLinks)). These VNs are anticipated to host services operating at hundreds of Gbps line-rate. As a consequence, even a short-lived network outage can cause a significant traffic disruption in these slices. However, ensuring reliability of network slices is non-trivial as failures in a transport network, such as transponder failure and fiber-cuts, are still the norm. A viable solution to ensure slice reliability is to pre-provision dedicated backup paths for each path used to embed the VLinks, also known as dedicated protection [7]. Dedicated backup paths can allow fast fail-over switching within milliseconds [8], but they incur a significant resource overhead since they remain idle during failure-free operations

In this paper, we propose a VN embedding solution with dedicated protection that incorporates two techniques to decrease the network-resource consumption: (i) bandwidth squeezing, *i.e.*, the opportunity to tune the amount of bandwidth guaranteed in case of failures [9]–[12]; and (ii) survivable multi-path provisioning [13], [14], *i.e.*, VLink demand splitting over multiple disjoint paths. Bandwidth squeezing is motivated by the fact that not all services require the full bandwidth to be operational, *e.g.*, a file transfer service can still be operational with reduced bandwidth during a failure. The extent of bandwidth reduction is measured by bandwidth squeezing rate (BSR), which is the percentage of original bandwidth made available after a failure. Survivable multi-path provisioning allows us to exploit the fact that not all of the disjoint splits belonging to the same VLink are jointly affected by a single substrate link failure. Therefore, the bandwidth of the surviving paths after a failure can be reused to provide a given BSR. Note that, in this paper, we consider a single substrate link failure scenario, which is more common than multiple simultaneous link failures [15].

The illustrative example in Fig. 1 demonstrates how the synergy of bandwidth squeezing and survivable multi-path provisioning can reduce backup resources for dedicated protection. If we do not allow any splitting of a VLink demand (*i.e.*, in our example, a 600Gbps demand is carried over a

This work was supported in part by Huawei Canada and in part by an NSERC Collaborative Research & Development (CRD) Grant. This work benefited from the use of CrySP RIPPLE Facility at University of Waterloo. Part of this work was presented at the 15th IEEE/ACM/IFIP International Conference on Network and Service Management (CNSM) 2019 [1]. The authors would like to thank the anonymous reviewers of IEEE/ACM/IFIP CNSM 2019 for their valuable feedback.

Nashid Shahriar (email: nshahria@uwaterloo.ca), Sepehr Taeb (email: staeb@uwaterloo.ca), Shihabur Rahman Chowdhury (email: sr2chowdhury@uwaterloo.ca), Mubeen Zulfiqar (email: mubeen.zulfiqar@uwaterloo.ca), and Raouf Boutaba (email: rboutaba@uwaterloo.ca) are with David R. Cheriton School of Computer Science, University of Waterloo, ON N2L 3G1, Canada.

Massimo Tornatore (email: massimo.tornatore@polimi.it) is with Politecnico di Milano, Milan, Italy.

Jeebak Mitra (email: jeebak.mitra@huawei.com) and Mahdi Hemmati (email: mahdi.hemmati@huawei.com) are with with Huawei Technologies Canada Research Center, Ottawa ON K2K 3J1, Canada.

This article has been accepted for publication in a future issue of this journal, but has not been fully edited. Content may change prior to final publication. Citation information: DOI 10.1109/TNSM.2020.2992442, IEEE Transactions on Network and Service Management

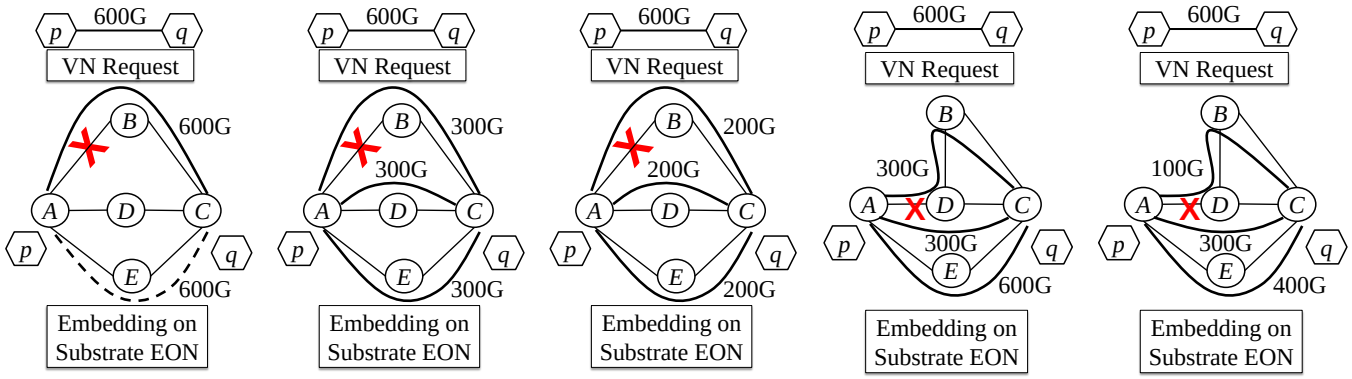

(a) No virtual link demand splitting (100% BSR) (b) Splitting over disjoint paths (100% BSR) (c) Splitting over disjoint paths (66% BSR) (d) Splitting over non-disjoint paths (100% BSR) (e) Splitting over non-disjoint paths (66% BSR)

Fig. 1. Benefits of virtual link demand splitting and the impact of availability of disjoint paths

single primary path A-B-C), then we require $2\times$ the original bandwidth for providing a dedicated protection path (A-E-C), as illustrated in Fig. 1(a). However, if we split the demand over three disjoint paths as in Fig. 1(b), then any two of the three paths will be active after a single substrate link failure. In this way 100% bandwidth will still be available after a failure, even though we are allocating a total bandwidth that is only $1.5\times$ the original demand. Bandwidth savings can even be higher if we employ bandwidth squeezing, *e.g.*, Fig. 1(c) shows how 66% BSR is ensured without any additional backup bandwidth. However, the advantages of multi-path provisioning depend on the availability of disjoint paths in the substrate network. For instance, the lack of sufficient number of disjoint paths reduces the gain of multi-path provisioning regardless of the extent of BSR as shown in Fig. 1(e) and Fig. 1(d).

In this paper, we present our solutions for reliable slicing of 5G transport networks based on VN embedding with dedicated protection over an EON. Our solutions leverage EON's capabilities in finer-grained spectrum allocation, adapting modulation format and Forward Error Correction (FEC) overhead for rightsize resource allocation to the VNs. We perform simulations using realistic network topologies, which provide valuable insight into how different levels of BSR and path diversity in the substrate EON impact the extent of backup resource savings for dedicated protection. We also analyze the steady state behavior of our heuristic solution using a discrete event simulator. For instance, our evaluation shows that by using multi-path provisioning it is possible to guarantee up to 40% of the requested bandwidth of a VN during failure (*i.e.*, $BSR \leq 40\%$) while using as low as 10% additional spectrum resources. Consequently, VN blocking ratio for $BSR \leq 40\%$ remains very similar to that of the case with no backup.

The rest of the paper is organized as follows. We discuss the relevant research literature in Section II and problem statement in Section III. Then, we formulate the optimal solution as an Integer Linear Program (ILP) in Section IV followed by a heuristic algorithm to solve large problem instances in Section V. In Section VI, we discuss the numerical evaluation of the proposed approaches over realistic network instances. Finally, we present our concluding remarks in Section VII.

II. Related Works

Reliability aspects of VN embedding [16] and, more generally, of traffic provisioning in fixed-grid optical networks [17] have been extensively studied. Techniques to enhance reliability [17] are typically categorized in two broad classes: protection and restoration. The first class contains proactive approaches where backup paths are provisioned at the time a VN or a traffic matrix is provisioned, which leads to faster recovery time. Backup paths can be either dedicated [18], [19] or shared among multiple requests [16], [20], [21]. In contrast, restoration techniques provision backup resources after a failure has occurred [22]. Restoration alleviates the issue of keeping a large amount of backup resources idle during regular operation, however it has significantly higher recovery time, not suitable for supporting ultra-reliable communications in 5G networks [17], [23], and will not be considered in this study. Similarly, shared protection could be used to reduce the amount of backup resources of dedicated protection [24]–[30], but at the cost of longer protections switching time [31], [32], hence in our study we focus on dedicated protection. In the following, we discuss the state-of-the-art research literature on VNE with dedicated protection and the literature on backup resource optimization techniques for VNE.

A. VNE with Dedicated Protection

Optical backbone networks have traditionally had very strict requirement on failure recovery time, typically in the order of few tens of milliseconds [17]. Such strict recovery time will continue to be the norm in 5G transport networks as well [8]. Fast failover within such short time can be achieved only through dedicated protection. Dedicated protection has its origin from survivable WDM optical networks where lightpaths are established with a dedicated backup path for quick recovery from fiber cuts [17]. In the context of 5G transport network slicing, dedicated protection can be in the form of providing dedicated protection to each virtual link of a network slice or VN. The concept of dedicated protection can be further extended to a whole VN topology as proposed in the research literature [33]. Ye *et al.*, address the dedicated VN topology protection problem by proposing a quadratic integer

This article has been accepted for publication in a future issue of this journal, but has not been fully edited. Content may change prior to final publication. Citation information: DOI 10.1109/TNSM.2020.2992442, IEEE Transactions on Network and Service Management

program and a greedy heuristic [18]. Later, Chowdhury *et al.*, modeled the VN topology protection problem as a variation of graph partitioning problem and proposed an ILP formulation to solve it optimally [19].

A weaker form of dedicated topology protection problem has been studied by Jiang *et al.*, [34]. The authors' proposed a scheme that embeds the backup virtual nodes disjointly from the primary virtual node embedding. However, the backup nodes can share substrate nodes among themselves, in this way reducing the degree of survivability. Also, they do not provision full bandwidth for the backup paths, rather, provision some backup paths in advance that can be used by the virtual links during failure.

The classical routing and spectrum allocation problem in EON with dedicated path protection has been addressed in [35]–[37]. However, the problem of reliable VNE over EON has gained attention only recently. Some research works have addressed the VN embedding problem over EON with dedicated path protection [38]–[40] while minimizing spectrum occupation, number of regenerators [38], [39] or energy consumption [40]. These works formulated the problem using a path-based ILP, where a disjoint backup path for each of the usable primary paths is pre-computed. Furthermore, they assume the modulation format is already selected for each bitrate (*e.g.*, 100Gbps bitrate is provisioned using only DP-QPSK modulation format), further limiting the solution space. In contrast, [41] proposed a modulation-adaptive link-disjoint path selection model by considering a step function based on realistic modulation formats in order to minimize the total number of utilized spectrum slots for dedicated protection.

Another protection technique for EONs is the use of *p-cycles* [42]–[44]. A p-cycle is a pre-configured cycle that act as a backup path for a link in the working paths of an EON. Unlike dedicated protection, backup p-cycles are needed for each EON link and recovery is performed locally in each EON link instead of providing end-to-end protection. As such backup spectrum requirement can be very high unless backup resources are shared among multiple working paths that, in consequence, may exceed the recovery time required by 5G transport network services. In this paper, we consider multi-path provisioning, bandwidth squeezing, and capture all the tunable transmission parameters made available by EONs, which is not considered by the existing works in the literature.

B. Backup resource optimization techniques for VNE

To save network resources, a number of studies considered a alternate form of protection, called bandwidth squeezing, where only a reduced bandwidth is guaranteed after a failure, according to a given BSR [9]–[12], [25], [45]. The advantages of using bandwidth squeezing can be amplified when combined with virtual link demand splitting over multiple disjoint substrate paths [9], [12], [46]. The latter is commonly known as survivable multi-path provisioning [13], [14], [45]–[47]. Majority of the survivable multi-path approaches, except [45], assume that all the paths used for embedding a virtual link are link disjoint, and may not explore the complete solution space. In addition, the authors in [48] proposed a scheme that consists in ensuring part of the minimum bitrate by protection as per BSR and complementing the rest by restoration. In contrast to these existing works, our work stands out by considering a VN topology embedding and by allowing splitting of a virtual link demand not only over non-disjoint paths but also over multiple spectral segments on the same path, significantly increasing the complexity of the problem as discussed in Section IV and V.

III. Mathematical Model and Problem Statement

We first present a mathematical model of the inputs followed by a formal statement of the problem. Without loss of generality, we assume the optical nodes to be colorless, directionless, and contentionless [49].

A. Substrate EON

The substrate EON (SN) is an undirected graph $G = (V, E)$, where V and E are the set of substrate optical nodes (SNodes) and substrate optical links (SLinks), respectively. We assume the SLinks to be bi-directional, *i.e.*, adjacent optical nodes are connected by one optical fiber in each direction. The optical frequency spectrum on each SLink $e = (u, v) \in E$ is divided into equal-width frequency slots represented by the set S and enumerated as $1, 2 \ldots |S|$. $\mathcal{P}$ and $\mathcal{P}^k_{uv} \subset \mathcal{P}$ represent the set of all paths in G and the set of k-shortest paths between nodes $u, v \in V$, respectively. The number of SLinks and the physical length of a path p in kilometers are represented by $|p|$ and $len(p)$, respectively. We use the binary variable δ_{pe} to denote the association between a path $p \in \mathcal{P}$ and an SLink $e \in E$.

The following transmission parameters can be configured on a path p with length $len(p)$ to enable data transmission with different data-rates $d \in \mathcal{D}$: *baud-rate* or *symbol-rate*, b, *modulation format*, m, and *FEC overhead*, f, selected from the set of possible values $\mathcal{B}$, $\mathcal{M}$, and $\mathcal{F}$, respectively. We use a tuple $t = (d, b, m, f) \in \mathcal{T} = (\mathcal{D} \times \mathcal{B} \times \mathcal{M} \times \mathcal{F})$ to represent a transmission configuration that dictates the combination of $b \in \mathcal{B}$, $m \in \mathcal{M}$, and $f \in \mathcal{F}$ yielding a data-rate $d \in \mathcal{D}$. We use $t^{(d)}, t^{(b)}, t^{(m)}$, and $t^{(f)}$ to denote the data-rate, baud-rate, modulation format, and FEC overhead of a configuration $t \in \mathcal{T}$. A *reach table* $\mathcal{R}$, computed based on physical layer characteristics, specifies the maximum length of a path (*i.e.*, the *reach* r_t) capable of retaining a satisfactory optical signal to noise ratio when configured according to a transmission configuration $t \in \mathcal{T}$. Finally, n_t denotes the number of slots required for a transmission configuration $t \in \mathcal{T}$, which is dependent on the parameters of t.

B. Virtual Network

The virtual network (VN) is represented by an undirected graph $\bar{G} = (\bar{V}, \bar{E})$, where $\bar{V}$ and $\bar{E}$ are the set of virtual nodes (VNodes) and virtual links (VLinks), respectively. The function $\tau : \bar{V} \rightarrow V$ represents VNode to SNode mapping and is an input to our problem (a common assumption for optical network virtualization [50]). Each virtual link $\bar{e} \in \bar{E}$ has a bandwidth requirement $\bar{\beta}_{\bar{e}}$ and a reliability requirement $0 < BSR_{\bar{e}} \leq 100$, which indicates the percentage of original bandwidth that should be available after an SLink fails.

This article has been accepted for publication in a future issue of this journal, but has not been fully edited. Content may change prior to final publication. Citation information: DOI 10.1109/TNSM.2020.2992442, IEEE Transactions on Network and Service Management

$BSR_{\bar{e}}$ can also be used to realize a bandwidth profile with a maximum and minimum demand similar to [6]. We allow VLinks to be mapped on multiple substrate paths (SPaths) (similar to [51], [52]), each with a lower data-rate than $\bar{\beta}_{\bar{e}}$. Splitting $\bar{\beta}_{\bar{e}}$ over multiple SPaths is a feasible way to support higher data-rates (*e.g.*, $\geq$ 400Gbps) that limit the number of usable paths due to their shorter reaches. However, we restrict the number of VLink splits to maximum q (≥ 1). Such multi-path embedding is supported by technologies such as Virtual Concatenation (VCAT) in Optical Transport Network (OTN) [53] or bonding capabilities of FlexEthernet [54].

C. Problem Statement

Given an SN G, a reach table $\mathcal{R}$, and a VN request $\bar{G}$ with given VNode mapping function τ.:

- Compute the link embedding function $\gamma : \bar{E} \rightarrow \chi : \chi \subset \mathcal{P} \times \mathcal{T} \times S^2$ and $1 \leq |\chi| \leq q$, *i.e.*, compute up to a maximum of q splits for each VLink $\bar{e} \in \bar{E}$ such that $0.01 \times BSR_{\bar{e}} \times \bar{\beta}_{\bar{e}}$ bandwidth is available during an SLink failure and at least $\bar{\beta}_{\bar{e}}$ bandwidth is available during the rest of the time. For each split, γ should select an SPath and an appropriate transmission configuration $t \in \mathcal{T}$ from the reach table $\mathcal{R}$, and allocate a contiguous segment of slots represented by the starting and ending slot index on each SLink along the SPath. Note that the same SPath can be used multiple times as the splits of a VLink following the reasoning in [52], [55]. $\chi_{\bar{e}i} = (p, t, s_b, s_t) | 1 \leq i \leq q$ represents the i-th split, where $\chi_{\bar{e}i}^{(p)}$ and $\chi_{\bar{e}i}^{(t)}$ denote the selected SPath and transmission configuration for the i-th split, respectively. In addition, allocation of spectrum slots for the i-th split begins at index $\chi_{\bar{e}i}^{(s_b)}$ and ends at index $\chi_{\bar{e}i}^{(s_t)}$ along each SLink in the SPath $\chi_{\bar{e}i}^{(p)}$.
- The total number of slots required to provision the VN is minimum according to the following cost function:

$$\sum_{\forall \bar{e} \in \bar{E}} \sum_{i=1}^{q} (\chi_{\bar{e}i}^{(s_t)} - \chi_{\bar{e}i}^{(s_b)} + 1) \times |\chi_{\bar{e}i}^{(p)}| \qquad (1)$$

  Here, $|\chi_{\bar{e}i}^{(p)}|$ is the number of SLinks on the SPath $\chi_{\bar{e}i}^{(p)}$.

The above is subject to substrate resource constraints, and spectral contiguity (*i.e.*, the allocated slots of each split are always adjacent to each other) and continuity (*i.e.*, the same sequence of slots are allocated on each SLink along an SPath) constraints on the lightpaths.

D. Pre-computations

For each VLink $\bar{e} \in \bar{E}$, we pre-compute $\mathcal{P}_{\bar{e}}^{k}$, a set of k shortest paths between the pair of SNodes where the VLink's endpoints' are mapped. For each SPath $p \in \mathcal{P}_{\bar{e}}^{k}$, we pre-compute the set of admissible transmission configurations, $\mathcal{T}_{\bar{e}p} \subset \mathcal{T}$, such that each configuration $t \in \mathcal{T}_{\bar{e}p}$ results in a reach $r_t \geq len(p)$ and has a data-rate $t^{(d)}$. $\mathcal{T}_{\bar{e}}$ contains all the distinct tuples suitable for $\bar{e}$ and is defined as $\bigcup_{\forall p \in \mathcal{P}_{\bar{e}}^{k}} \mathcal{T}_{\bar{e}p}$.

TABLE I
NOTATION TABLE

Inputs & Pre-computations	
$G = (V, E)$	Substrate EON
$G = (V, E)$	Virtual Network (VN)
S	The set of equal-width frequency slots
$\mathcal{P}$	Set of all paths in G
$\mathcal{P}_{uv}^{k} \subset \mathcal{P}$	k-shortest paths between u and v in G
$\mathcal{D}, \mathcal{B}, \mathcal{M}, \mathcal{F}$	Set of all possible data-rates, baud-rates, modulation formats, & FEC overhead levels
$\mathcal{T} = (\mathcal{D} \times \mathcal{B} \times \mathcal{M} \times \mathcal{F})$	Set of all possible transmission configs
$t = (d, b, m, f) \in \mathcal{T}$	A transmission config. *i.e.*, a baud-rate b, modulation format m, and FEC overhead f yielding data-rate d
$t^{(d)} \in \mathcal{D}, t^{(b)} \in \mathcal{B}$, $t^{(m)} \in \mathcal{M}, t^{(f)} \in \mathcal{F}$	data-rate, baud-rate, modulation format, and FEC overhead of transmission config. t
$\mathcal{R}$	Reach table
$r_t \in \mathcal{R}$	Achievable reach for config. t
n_t	No. of slices required for config. t
$\mathcal{P}_{\bar{e}}^{k}$	k candidate shortest paths for VLink $\bar{e} \in \bar{E}$
$\mathcal{T}^{\bar{e}p} \subset \mathcal{T}$	Admissible transmission configs on path p for embedding VLink $\bar{e} \in \bar{E}$
Decision Variables	
$w_{\bar{e}pti}$	Indicates if $\bar{e} \in \bar{E}$ uses i-th instance of transmission config. $t \in \mathcal{T}_{\bar{e}p}$ on $p \in \mathcal{P}_{\bar{e}}^{k}$
$y_{\bar{e}ptis}$	Indicates if $\bar{e} \in E$ uses slot $s \in S$ on $p \in \mathcal{P}_{\bar{e}}^{k}$ with the i-th instance of transmission config. $t \in \mathcal{T}_{\bar{e}p}$

IV. Problem Formulation

We present a path-based ILP formulation for optimally solving our problem. Note that some of the constraints, except the reliability constraints, have been presented in different forms in different research works [52], [56], [57]. In the interest of completeness, we report all the constraints in the following. Table I presents a glossary of key notation used in the ILP formulation.

A. Decision Variables

We allow a VLink's bandwidth demand to be satisfied by provisioning spectrum slots over one or more SPaths where an SPath can be used more than once (up to a maximum of q) as discussed in III-C. To model the same SPath appearing more than once in a VLink's embedding, we assume each transmission configuration on an SPath can be instantiated multiple times (up to a maximum of q times). The following variable represents VLink mapping:

$$w_{\bar{e}pti} = \begin{cases} 1 & \text{if } \bar{e} \in \bar{E} \text{ uses } i\text{-th instance of } t \in \mathcal{T}_{\bar{e}p} \\ & \text{on path } p \in \mathcal{P}_{\bar{e}}^{k} \\ 0 & \text{otherwise} \end{cases}$$

Finally, the following decision variable creates the relationship between a mapped SPath and the slots in its SLinks:

$$y_{\bar{e}ptis} = \begin{cases} 1 & \text{if } \bar{e} \in \bar{E} \text{ uses slot } s \in S \text{ on path } p \in \mathcal{P}_{\bar{e}}^{k} \\ & \text{with the } i\text{-th instance of } t \in \mathcal{T}_{\bar{e}p} \\ 0 & \text{otherwise} \end{cases}$$

B. Constraints

1) VLink demand constraints: We provision a VLink by splitting it across multiple (up to q) SPaths. Each of these splits

This article has been accepted for publication in a future issue of this journal, but has not been fully edited. Content may change prior to final publication. Citation information: DOI 10.1109/TNSM.2020.2992442, IEEE Transactions on Network and Service Management

are then assigned a transmission configuration, resulting in provisioning a data-rate along the split. Constraint (2) ensures that for each VLink $\bar{e} \in \bar{E}$, the sum of data-rates resulting from applying the selected transmission configuration on the selected splits is equal or larger than the VLink's demand. (3) enforces an upper limit on the number of splits in order to keep splitting overhead within a operator defined threshold.

$$\forall \bar{e} \in \bar{E} : \bar{\beta}_{\bar{e}} \leq \sum_{\forall p \in \mathcal{P}_{\bar{e}}^k} \sum_{\forall t \in \mathcal{T}_{\bar{e}p}} \sum_{i=1}^{q} (w_{\bar{e}pti} \times t^{(d)}) \tag{2}$$

$$\forall \bar{e} \in \bar{E} : \sum_{\forall p \in \mathcal{P}_{\bar{e}}^k} \sum_{\forall t \in \mathcal{T}_{\bar{e}p}} \sum_{i=1}^{q} w_{\bar{e}pti} \leq q \tag{3}$$

2) Slot assignment and Spectral Contiguity constraints: We ensure by (4) that if a path p is selected with a specific transmission configuration t, then the required number of slots n_t to support the data-rate $t^{(d)}$ is allocated on the path. Then, (5) ensures that each slot on an SLink is allocated to at most one path. Finally, (6) enforces spectrum contiguity constraint [52], *i.e.*, ensures the slots allocated on each SLink of a path form a contiguous frequency spectrum.

$$\forall \bar{e} \in \bar{E}, \forall p \in \mathcal{P}_{\bar{e}}^k, \forall t \in \mathcal{T}_{\bar{e}p}, 1 \leq i \leq q : \sum_{\forall s \in S} y_{\bar{e}ptis} = n_t w_{\bar{e}pti} \tag{4}$$

$$\forall e \in E, \forall s \in S : \sum_{\forall \bar{e} \in \bar{E}} \sum_{\forall p \in \mathcal{P}_{\bar{e}}^k} \sum_{\forall t \in \mathcal{T}_{\bar{e}p}} \sum_{i=1}^{q} w_{\bar{e}pti} y_{\bar{e}ptis} \delta_{pe} \leq 1 \tag{5}$$

$$\forall \bar{e} \in \bar{E}, \forall p \in \mathcal{P}_{\bar{e}}^k, \forall t \in \mathcal{T}_{\bar{e}p}, 1 \leq i \leq q, 1 \leq s \leq |S| - 1 : \sum_{s'=s+2}^{|S|} y_{\bar{e}ptis'} \leq |S| \times (1 - y_{\bar{e}ptis} + y_{\bar{e}pti(s+1)}) \tag{6}$$

3) Reliability constraints: We must ensure that for each single substrate link failure scenario, the sum of data-rates of the unaffected splits of a VLink $\bar{e} \in \bar{E}$ is at least $BSR_{\bar{e}}$ percentage of the original VLink demand. This is enforced by (7) as follows:

$$\forall \bar{e} \in \bar{E}, \forall e \in E : (\sum_{\forall p \in \mathcal{P}_{\bar{e}}^k} \sum_{\forall t \in \mathcal{T}_{\bar{e}p}} \sum_{i=1}^{q} w_{\bar{e}pti} t^{(d)}) - (\sum_{\forall p \in \mathcal{P}_{\bar{e}}^k} \sum_{\forall t \in \mathcal{T}_{\bar{e}p}} \sum_{i=1}^{q} w_{\bar{e}pti} t^{(d)} \delta_{pe}) \geq 0.01 BSR_{\bar{e}} \bar{\beta}_{\bar{e}} \tag{7}$$

C. Objective Function

Our cost function minimizes the total number of spectrum slots required to embed all the VLinks of a VN as shown in the first part of (8). However, to break ties among multiple solutions with the same total number of slots, we use the second term with a fractional weight ϵ in (8). This term minimizes the number of splits over all the VLinks since each split requires a pair of transponders at the source and destination node of a lightpath. This gives us the following objective function:

$$\text{minimize}(\sum_{\forall \bar{e} \in \bar{E}} \sum_{\forall p \in \mathcal{P}_{\bar{e}}^k} \sum_{\forall t \in \mathcal{T}_{\bar{e}p}} \sum_{i=1}^{q} \sum_{\forall s \in S} y_{\bar{e}ptis} |p| + \epsilon \sum_{\forall \bar{e} \in \bar{E}} \sum_{\forall p \in \mathcal{P}_{\bar{e}}^k} \sum_{\forall t \in \mathcal{T}_{\bar{e}p}} \sum_{i=1}^{q} w_{\bar{e}pti}) \tag{8}$$

D. Complexity of the ILP

The problem of VN embedding on EON with dedicated path protection and multi-path provisioning is reducible to routing and spectrum allocation in EON, which is known to be NP-hard [58]. This also makes the problem addressed in this paper NP-hard. The complexity of an ILP solution for optimally solving a problem will depend on the number of variables and constraints in the formulation. In case of our formulation, it will require enumerating $O(|\bar{E}|\mathcal{P}\mathcal{T}qS)$ variables while considering $O(|S||E| + |S||\bar{E}|\mathcal{P}\mathcal{T}q)$ constraints.

V. Heuristic Algorithm

Given the limited scalability of the ILP formulation, we develop a heuristic algorithm to solve large instances of our problem. In this section, we first give an overview of the main steps involved in reliable VN embedding for a given node mapping (Section V-A). Then, we discuss how we select the order of VLinks to be embedded for increasing the chances of finding a feasible solution (Section V-B). Finally, we discuss the embedding process of a single VLink (Section V-C).

A. Heuristic Solution for Reliable VN Embedding

Algorithm 1: Compute VN Embedding

```
1  function EmbedVN(G, Ḡ, τ)
2      Ē ← GetVLinkOrder(G, Ḡ)
3      foreach ē ∈ Ē in the sorted order do
4          I_ē ←FindEmbedding(G, ē, P^i_ē, T_ē)
5          foreach e ∈ p|p ∈ I_ē.ℙ do
6              Perform slot assignment using I_ē.S
7          χ_ē.P ← I_ē.ℙ, χ_ē.T ← I_ē.𝕋_ℙ
8          if χ_ē = φ then
9              return < φ, φ >
10     return < τ : V̄ → V, γ : Ē → χ >
```

Alg. 1 takes as input a VN $\bar{G}$, an EON G, and a node mapping function $\tau : \bar{V} \rightarrow V$. One way of computing a cost efficient VLink mapping for a given VNode mapping is to consider all $|\bar{E}|!$ possible orders for sequentially embedding VLinks. The lowest cost mapping among all possible VLink orders then can be chosen as a cost effective solution for the given VNode mapping. However, this brute-force approach is not scalable. Instead, Alg. 1 considers only one sequential VLink order that is computed to converge to a solution within a reasonable time. To increase the chances of finding a feasible VN embedding, Alg. 1 invokes Alg. 2 that finds a good order of the VLinks ($\bar{\mathcal{E}}$) to embed. For each VLink $\bar{e} \in \bar{\mathcal{E}}$ in the

This article has been accepted for publication in a future issue of this journal, but has not been fully edited. Content may change prior to final publication. Citation information: DOI 10.1109/TNSM.2020.2992442, IEEE Transactions on Network and Service Management

computed order, Alg. 1 finds the embedding solution based on $\mathcal{P}_{\bar{e}}^{i}$ by invoking Alg. 3 (line 4). Alg. 1 then allocates spectrum slots on all SLinks present in the solution and updates the VLink embedding $\chi_{\bar{e}}$ accordingly. If no such solution for $\bar{e}$ can be found, the embedding of the VN is rejected.

B. Compute VLink Ordering

Algorithm 2: Find a VLink embedding order

1 **function** *GetVLinkOrder*$(G, \bar{G})$
2 $Z = (N, A) \leftarrow$ AuxGraph($\bar{G}$), $O[1...n] \leftarrow \phi$, $i \leftarrow n$
3 **while** $N \neq \phi$ **do**
4 **foreach** $n_{\bar{e}_i} \in N$ **do**
5 Compute $w(n_{\bar{e}_i})$ using (12)
6 $n_{\bar{e}_i}^{min} \leftarrow n_{\bar{e}_i}$ with minimum $w(n_{\bar{e}_i})$
7 $O[i] \leftarrow \bar{e}_i$ corresponding to $n_{\bar{e}_i}^{min}$
8 $N \leftarrow N - \{n_{\bar{e}_i}\}$
9 **foreach** $(n_{\bar{e}_i}^{min}, n_{\bar{e}_j}) \in A$ **do**
$A \leftarrow A \setminus \{(n_{\bar{e}_i}^{min}, n_{\bar{e}_j})\}$
10 $i \leftarrow i - 1$
11 **return** O

Alg. 2 finds an order of VLinks, O, that increases the chances of finding a feasible embedding for all the VLinks. Computing a feasible embedding of a VLink depends on the availability of contiguous slots in the candidate SPaths of that VLink. If the candidate SPaths $\mathcal{P}_{\bar{e}_i}^{k}$ of a VLink $\bar{e}_i$ have many SLinks that are common with the candidate SPaths of other VLinks that appear before $\bar{e}_i$ in a VLink order o, the slots of these SLinks (correspondingly, SPaths) may be exhausted or fragmented in such a way that the embedding of $\bar{e}_i$ becomes infeasible. Note that VLinks that come after $\bar{e}_i$ in o do not have any impact on the embedding of $\bar{e}_i$ even though $\bar{e}_i$ and the VLinks after $\bar{e}_i$ have common SLinks in their candidate SPath sets. Hence, effective commonality of $\bar{e}_i$ depends on o and is defined as follows:

$$w(\bar{e}_i)^o = \sum_{\bar{e}_j \text{ precedes } \bar{e}_i \text{ in } o | \bar{e}_i \in \bar{E},\ \bar{e}_j \in \bar{E},\ \bar{e}_i \neq \bar{e}_j} w(\bar{e}_i, \bar{e}_j) \tag{9}$$

where, $w(\bar{e}_i, \bar{e}_j)$ is the commonality between two VLinks $\bar{e}_i$ and $\bar{e}_j$ irrespective of any order and is defined as follows:

$$w(\bar{e}_i, \bar{e}_j) = |\{(p_{\bar{e}_i}, p_{\bar{e}_j}) : (p_{\bar{e}_i}, p_{\bar{e}_j}) \in \mathcal{P}_{\bar{e}_i}^{k} \times \mathcal{P}_{\bar{e}_j}^{k} \wedge p_{\bar{e}_i} \cap p_{\bar{e}_j} \neq \phi\}| \tag{10}$$

A high value of $w(\bar{e}_i, \bar{e}_j)$ indicates more SPath pairs from the candidate SPath sets of $\bar{e}_i$ and $\bar{e}_j$ have common SLinks. Using (9), we define the commonality index of o as follows:

$$w^o = \max_{\bar{e}_i \in \bar{E}} w(\bar{e}_i)^o \tag{11}$$

To increase the chances of finding a feasible embedding for all the VLinks, Alg. 2 finds an order O that minimizes w^o for all possible orders of $\bar{E}$. To do so, Alg. 2 first constructs an auxiliary graph $Z = (N, A)$ based on a VN $\bar{G}$ and EON G (lines 2). The auxiliary graph $Z = (N, A)$ is a weighted undirected graph where N is the set of nodes and A is the set of edges. There is a one-to-one correspondence between a node $n_{\bar{e}_i} \in N$ and a VLink $\bar{e}_i \in \bar{E}$. Therefore, an order of the nodes in N corresponds to an order of the VLinks in $\bar{E}$. We include a weighted edge $(n_{\bar{e}_i}, n_{\bar{e}_j}) \in A$ between two distinct nodes $n_{\bar{e}_i} \in N$ and $n_{\bar{e}_j} \in N$ with weight $w(\bar{e}_i, \bar{e}_j)$. Using (10), we define the weight of a node $n_{\bar{e}_i} \in N$ as follows:

$$w(n_{\bar{e}_i}) = \sum_{n_{\bar{e}_j} | (n_{\bar{e}_i}, n_{\bar{e}_j}) \in A} w(\bar{e}_i, \bar{e}_j) \tag{12}$$

To compute a node order (or a corresponding VLink order) that minimizes w^o, Alg. 2 iteratively computes $w(n_{\bar{e}_i})$ using (12) for all the nodes in N. Then Alg. 2 chooses the node $n_{\bar{e}_i}^{min}$ with the minimum weight $w(n_{\bar{e}_i})$ and inserts the corresponding VLink to the last empty spot in the VLink order O (line 15). Afterwards, the algorithm updates Z by removing $n_{\bar{e}_i}^{min}$ and all of its incident edges. The updated auxiliary graph Z allows us to use (12) to compute $w(n_{\bar{e}_i})$ that corresponds to $w(\bar{e}_i)^O$ as updated Z now only have all the nodes (and adjacent edges) that precede $n_{\bar{e}_i}^{min}$ in the node order, or equivalently $\bar{e}_i^{min}$ in O. Alg. 2 repeats this process until all the VLinks are added to O.

Theorem 1. *Alg. 2 returns a VLink ordering with the minimum commonality index.*

Proof. Suppose VLink ordering o which is generated by Alg. 2 does not have the minimum commonality index, therefore, there exists a VLink ordering o^* for which $w^o > w^{o^*}$. Let $\bar{e}_1^o, \bar{e}_2^o, ..., \bar{e}_{|\bar{E}|}^o$ and $\bar{e}_1^{o^*}, \bar{e}_2^{o^*}, ..., \bar{e}_{|\bar{E}|}^{o^*}$ denote the VLink ordering o and o^* respectively. Since $w^o \neq w^{o^*}$ there exists at least one index i for which $\bar{e}_j^o$ and $\bar{e}_j^{o^*}$ are not corresponding to the same VLink. Let i_{max} be the maximum index with this condition. Since both VLink ordering o and o^* contain all the VLinks, there should be an index j such that $\bar{e}_j^{o^*}$ corresponds to the same VLink as $\bar{e}_{i_{max}}^o$. We create a new VLink ordering o_1^* by moving the $\bar{e}_j^{o^*}$ to the i_{max}th index in the o^* VLink ordering (Fig. 2).

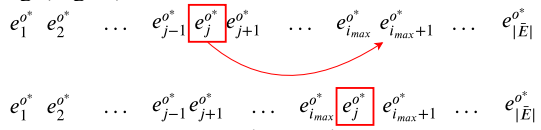

Fig. 2. Creating VLink ordering o_1^* from o^*

Lemma 1. *The commonality index of VLink ordering o_1^* is less than or equal to the commonality index of the VLink ordering o^* ($w^{o_1^*} \leq w^{o^*}$).*

Proof. We divide the proof of the lemma in two parts. At first, we prove *i)* the effective commonality of all the VLinks (except $\bar{e}_j^{o^*}$) in VLink ordering o_1^* is less than or equal to the effective commonality of the same VLink in VLink ordering o^*, i.e. $\forall \bar{e}_i \in \bar{E} - \{\bar{e}_j^{o^*}\} : w(\bar{e}_i)^{o_1^*} \leq w(\bar{e}_i)^{o^*}$. Then we prove *ii)* $w(\bar{e}_j^{o^*})^{o_1^*} \leq w(\bar{e}_{i_{max}}^{o^*})^{o^*}$, hence, for each VLink in VLink ordering o_1^* there exists at least one VLink in VLink ordering o^* such that its effective commonality is greater or equal, i.e. $\forall \bar{e}_i \in \bar{E}, \exists \bar{e}_j : w(\bar{e}_i)^{o_1^*} \leq w(\bar{e}_j)^{o^*}$. From (11), the commonality index of a VLink ordering is equal to the maximum effective commonality of all VLinks in that ordering, therefore, $w^{o_1^*} \leq w^{o^*}$.

This article has been accepted for publication in a future issue of this journal, but has not been fully edited. Content may change prior to final publication. Citation information: DOI 10.1109/TNSM.2020.2992442, IEEE Transactions on Network and Service Management

To prove *i)*, we divide VLinks into 3 groups (Fig. 3):

1) $A = \{\bar{e}_i^{o^*} | 1 \leq i < j\}$ which includes all the VLinks that come before $\bar{e}_j^{o^*}$ in both o^* and o_1^*.
2) $B = \{\bar{e}_i^{o^*} | j < i \leq i_{max}\}$ which contains all the VLinks that come after $\bar{e}_j^{o^*}$ in o^*, but before $\bar{e}_j^{o^*}$ in o_1^*.
3) $C = \{\bar{e}_i^{o^*} | i_{max} < i \leq |\bar{E}|\}$ which includes the VLinks that come after $\bar{e}_j^{o^*}$ in both o^* and o_1^*.

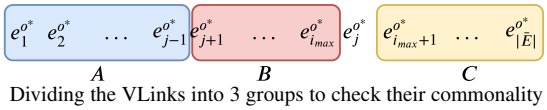

Fig. 3. Dividing the VLinks into 3 groups to check their commonality indexes

From (9), we know that the effective commonality of each VLink only depends on the preceding VLinks. Hence, considering that the set of preceding VLinks is the same $\forall \bar{e}_i \in A \cup C$ in ordering o^* and o_1^*, their effective commonalities are the same, i.e. $\forall \bar{e}_i \in A \cup C : w(\bar{e}_i^{o^*})^{o_1^*} = w(\bar{e}_i^{o^*})^{o^*}$. In addition, the set of preceding VLinks of $\bar{e}_i \in B$ in o_1^* is the same as their set of preceding VLinks in o^* minus $\bar{e}_j^{o^*}$. Therefore, $\forall \bar{e}_i \in B : w(\bar{e}_i)^{o_1^*} = w(\bar{e}_i)^{o^*} - w(\bar{e}_i, \bar{e}_j^{o^*}) \leq w(\bar{e}_i)^{o^*}$.

For proving *ii)*, we need to show that $w(\bar{e}_j^{o^*})^{o_1^*} \leq w(\bar{e}_{i_{max}}^{o^*})^{o^*}$. Recall that Alg. 2, at each iteration, finds the VLink with minimum weight and puts it at the first empty place at the end of ordering (Line 4–7). Since the ordering o, which is generated by Alg. 2, is identical to ordering o^* from index $i_{max}+1$ to $\bar{E}$, it means that VLink $\bar{e}_j^o = \bar{e}_{i_{max}}^{o^*}$ has the minimum weight, therefore $w(n_{\bar{e}_j^o}) \leq w(n_{\bar{e}_{i_{max}}^{o^*}})$ at $(n - i_{max} + 2)$-th step (to find the VLink that should be at index i_{max}). Since (12) computes the effective commonality of the all the remaining VLinks assuming they will be at the last empty spots $w(n_{\bar{e}_j^o}) = w(\bar{e}_j^{o^*})^{o_1^*}$ and $w(n_{\bar{e}_{i_{max}}^{o^*}}) = w(\bar{e}_{i_{max}}^{o^*})^{o^*}$. So $w(\bar{e}_j^{o^*})^{o_1^*} \leq w(\bar{e}_{i_{max}}^{o^*})^{o^*}$.

By showing these two parts, we prove that $w^{o_1^*} \leq w^{o^*}$. □

We start from VLink ordering $o_0^* = o^*$ and at ith step we generate o_i^* from o_{i-1}^* using the same approach to generate o_1^* from o^*. Since the maximum index for which o_1^* and o are different decreases after each step, finally, after $s \leq |\bar{E}|$ steps, $o = o_s^*$. By Lemma 1 we know that the commonality index does not increase after each step, i.e., $w^{o_i^*} \leq w^{o_{i-1}^*}$. Therefore $w^o = w^{o_s^*} \leq w^{o^*}$, which contradicts the initial assumption. This means that Alg. 2 returns an ordering with the minimum commonality index. □

C. Compute Embedding of a Single VLink

The embedding of a VLink computed by Alg. 3 consists of a multi-set of SPaths where each SPath in the multi-set has an associated transmission configuration and spectrum slot allocation. Recall from Section I that bandwidth requirement for dedicated protection against single SLink failure for a VLink depends on BSR and the number of disjoint SPaths used in the multi-set of SPaths of a solution. To exploit disjointness of the SPaths in the candidate SPath set $\mathbb{P}_{\bar{e}}^k$ of a VLink $\bar{e}$, Alg. 3 first computes disjoint SPath groups from the SPaths in $\mathbb{P}_{\bar{e}}^k$. We define a disjoint SPath group $H_{\bar{e}}$ from $\mathcal{P}_{\bar{e}}^k$ as follows:

$$H_{\bar{e}} = \{\delta\mathcal{P}_{\bar{e}}^k | \delta\mathcal{P}_{\bar{e}}^k \subseteq \mathcal{P}_{\bar{e}}^k \text{and } |\delta\mathcal{P}_{\bar{e}}^k| > 1 \text{ and the SPaths in } \delta\mathcal{P}_{\bar{e}}^k \text{ are link disjoint}\} \quad (13)$$

Note that two SPaths belonging to two different disjoint SPath groups $H_{\bar{e}}^i$ and $H_{\bar{e}}^j$ may share an SLink and an SPath can appear in multiple disjoint SPath groups. The set of all disjoint SPath groups for a VLink $\bar{e}$ is denoted by $\mathcal{H}_{\bar{e}}$. For instance, in Fig. 1(a), $\mathcal{H}_{\bar{p}\bar{q}} = \{\{AB - BC, AD - DC\}, \{AB - BC, AE - EC\}, \{AD - DC, AE - EC\}, \{AB - BC, AD - DC, AE - EC\}\}$, and in Fig. 1(e), $\mathcal{H}_{\bar{p}\bar{q}} = \{\{AD - DC, AE - EC\}, \{AD - DB - BC, AE - EC\}\}$.

Alg. 3 needs to enumerate all non-empty subsets of $\mathcal{H}_{\bar{e}}$ to find the optimal solution. Such enumeration is not scalable as the number of subsets of $\mathcal{H}_{\bar{e}}$ grows exponentially with the size of $\mathcal{H}_{\bar{e}}$. Hence, Alg. 3 applies a heuristic to obtain a smaller set of disjoint SPath groups $\mathbb{H}_{\bar{e}} \subseteq \mathcal{H}_{\bar{e}}$ that includes the most probable SPaths to be used as the splits of $\bar{e}$. The heuristic is motivated by the fact that longer SPaths allow only lower order modulation formats with a higher FEC that may require a large number of spectrum slots. In addition, longer SPaths often consist of more intermediate hops, thus increasing the total spectrum usage as per (8). To exclude such longer SPaths, our heuristic should construct $\mathbb{H}_{\bar{e}}$ with those disjoint SPath groups whose average total distances are small. However, doing so may bias the algorithm to include disjoint SPath groups with smaller number of SPaths for keeping the average distance low, which can reduce the benefits of splitting over multiple disjoint paths. Alg. 3 circumvents this issue by considering disjoint SPath groups of all sizes. From each set of disjoint SPath groups with size i, Alg. 3 selects the first σ disjoint SPath groups ranked by the increasing average distance of the group (Line 6–9). The value of σ is an input to Alg. 3 that can be used to keep the size of $\mathbb{H}_{\bar{e}}$ small.

After computing $\mathbb{H}_{\bar{e}}$, Alg. 3 enumerates all non-empty subsets of $\mathbb{H}_{\bar{e}}$ to assign data-rates to each disjoint SPath group in the subset such that each group provides dedicated protection as per BSR requirement for its data-rate. For each subset $\delta\mathbb{H}_{\bar{e}} \subseteq \mathbb{H}_{\bar{e}}$, Alg. 3 selects $|\delta\mathbb{H}_{\bar{e}}|$ data-rates such that the sum of these data-rates equals to demand $\bar{\beta}_{\bar{e}}$ (Line 10). These combinations of data-rates is represented by a multi-set $\mathbb{D}_{\delta\mathbb{H}_{\bar{e}}} = (\mathcal{D}, m_1)$, where $\mathcal{D}$ is the set of all data-rates, and $m_1 : \mathcal{D} \rightarrow N$ is the number of times a data-rate in $\mathcal{D}$ appears in $\mathbb{D}_{\delta\mathbb{H}_{\bar{e}}}$. $\mathcal{M}(\mathbb{D}_{\delta\mathbb{H}_{\bar{e}}})$ represents all possible multi-sets of $\mathbb{D}_{\delta\mathbb{H}_{\bar{e}}}$.

Since none of $\delta\mathbb{H}_{\bar{e}}$ and $\mathbb{D}_{\delta\mathbb{H}_{\bar{e}}}$ are ordered sets, Alg. 3 needs to enumerate all permutations of data-rates from $\mathbb{D}_{\delta\mathbb{H}_{\bar{e}}}$ to assign data-rates in $\mathbb{D}_{\delta\mathbb{H}_{\bar{e}}}$ to $|\delta\mathbb{H}_{\bar{e}}|$ SPath groups. To do so, Alg. 3 generates all permutations of data-rates for each multi-set $\mathbb{D}_{\delta\mathbb{H}_{\bar{e}}} \in \mathcal{M}(\mathbb{D}_{\delta\mathbb{H}_{\bar{e}}})$, denoted by $\zeta(\mathbb{D}_{\delta\mathbb{H}_{\bar{e}}})$ (Line 12). For each of these permutations of data-rates $\mathrm{D}_{\delta\mathbb{H}_{\bar{e}}} \in \zeta(\mathbb{D}_{\delta\mathbb{H}_{\bar{e}}})$, Alg. 3 assigns a data-rate $d_{H_{\bar{e}}}$ from $\mathrm{D}_{\delta\mathbb{H}_{\bar{e}}}$ to a disjoint SPath group $H_{\bar{e}} \in \delta\mathbb{H}_{\bar{e}}$ in the same order (Line 15). For each disjoint SPath group $H_{\bar{e}} \in \delta\mathbb{H}_{\bar{e}}$ with its assigned data-rate $d_{H_{\bar{e}}}$, the algorithm computes the data-rate $d_{p_{H_{\bar{e}}}}$ of an SPath $p \in H_{\bar{e}}$ using (14) that takes into account the number of disjoint SPaths in $H_{\bar{e}}$ and $BSR_{\bar{e}}$ of the VLink (Line 16). $d_{p_{H_{\bar{e}}}}$ is computed in a way such that the SPaths in $H_{\bar{e}}$ protect $BSR_{\bar{e}}$ fraction of $d_{H_{\bar{e}}}$ under any single SLink failure. However, when $BSR_{\bar{e}}$ is low, protection requirement is not enough to provide the assigned data-rate $d_{H_{\bar{e}}}$. In this case, data-rate $d_{p_{H_{\bar{e}}}}$ for an SPath is computed by equally dividing $d_{H_{\bar{e}}}$ along each disjoint SPath in $H_{\bar{e}}$. Note

This article has been accepted for publication in a future issue of this journal, but has not been fully edited. Content may change prior to final publication. Citation information: DOI 10.1109/TNSM.2020.2992442, IEEE Transactions on Network and Service Management

that each SPath in $H_{\bar{e}}$ will have an equal data-rate $d_{p_{H_{\bar{e}}}}$.

$$d_{p_{H_{\bar{e}}}} = max(\frac{d_{H_{\bar{e}}} \times BSR_{\bar{e}}}{100 \times (|H_{\bar{e}}| - 1)}, \frac{d_{H_{\bar{e}}}}{|H_{\bar{e}}|}) \quad (14)$$

Since an SPath p can appear in multiple disjoint SPath groups in $\delta\mathbb{H}_{\bar{e}}$, a consolidation step is introduced to compute the total data-rate assigned to p (denoted by $d_{p_{\delta\mathbb{H}_{\bar{e}}}}$) using (15) (Line 17). Since the possible data-rates in the reach table are discrete values, the ceiling function returns the nearest rounded up data-rate after the summation in (15).

$$d_{p_{\delta\mathbb{H}_{\bar{e}}}} = \left\lceil \sum_{\forall H_{\bar{e}} \in \delta\mathbb{H}_{\bar{e}}} d_{p_{H_{\bar{e}}}} \right\rceil \quad (15)$$

After the consolidation step, we get a set of distinct (not necessarily disjoint) SPaths $P_{\delta\mathbb{H}_{\bar{e}}}$ and their assigned data-rates for a particular $\delta\mathbb{H}_{\bar{e}}$ and $\mathbb{D}_{\delta\mathbb{H}_{\bar{e}}}$. However, an SPath $p_{\delta\mathbb{H}_{\bar{e}}} \in P_{\delta\mathbb{H}_{\bar{e}}}$ may split its assigned data-rate $d_{p_{\delta\mathbb{H}_{\bar{e}}}}$ into smaller data-rates either to ensure spectrum contiguity or to minimize the number of slots. To enumerate these possibilities, Alg. 3 generates the set of all possible multi-sets $\mathcal{M}(\mathbb{P}_{\delta\mathbb{H}_{\bar{e}}})$ out of the set $P_{\delta\mathbb{H}_{\bar{e}}}$ (Line 18). A multi-set $\mathbb{P}_{\delta\mathbb{H}_{\bar{e}}} \in \mathcal{M}(\mathbb{P}_{\delta\mathbb{H}_{\bar{e}}})$ is defined as $\mathbb{P}_{\delta\mathbb{H}_{\bar{e}}} = (P_{\delta\mathbb{H}_{\bar{e}}}, m_2)$, where, $m_2 : P_{\delta\mathbb{H}_{\bar{e}}} \rightarrow N$ is the number of times an SPath in $P_{\delta\mathbb{H}_{\bar{e}}}$ appears in $\mathbb{P}_{\delta\mathbb{H}_{\bar{e}}}$. For each multi-set $\mathbb{P}_{\delta\mathbb{H}_{\bar{e}}}$, Alg. 3 assigns data-rates to each instance of SPath in $\mathbb{P}_{\delta\mathbb{H}_{\bar{e}}}$. This is trivial for an SPath that appears once in $\mathbb{P}_{\delta\mathbb{H}_{\bar{e}}}$ ($m_2(p) = 1$). For an SPath with $m_2(p) > 1$, Alg. 3 distributes the assigned data-rate $d_{p_{\delta\mathbb{H}_{\bar{e}}}}$ into $m_2(p)$ splits by generating permutations of multi-sets of data-rates of size $m_2(p)$ (Line 21–23). To get the set of all data-rate permutations $\mathcal{M}(\mathrm{D}_{\mathbb{P}_{\delta\mathbb{H}_{\bar{e}}}})$ for $\mathbb{P}_{\delta\mathbb{H}_{\bar{e}}}$, Alg. 3 considers all possible ways to combine the data-rate permutations of each distinct SPath in $P_{\delta\mathbb{H}_{\bar{e}}}$ (Line 24).

Once we have an SPath multi-set $\mathbb{P}_{\delta\mathbb{H}_{\bar{e}}}$ and its data-rate permutation $\mathrm{D}_{\mathbb{P}_{\delta\mathbb{H}_{\bar{e}}}}$, Alg. 3 invokes MDP procedure to find feasible transmission configuration and spectrum slot allocation with the least slot requirement (Line 26). MDP procedure is adapted from [52] that first selects a transmission configuration to achieve a data-rate in $\mathrm{D}_{\mathbb{P}_{\delta\mathbb{H}_{\bar{e}}}}$ along an SPath in $\mathbb{P}_{\delta\mathbb{H}_{\bar{e}}}$ and allocates the slots required by the transmission configuration using First-fit [58]. Among all the feasible solutions returned by MDP procedure, Alg. 3 selects the one that minimizes (8).

1) Running Time Analysis: Alg. 3 explores all subsets of $\mathbb{H}_{\bar{e}}$ yielding $2^{|\mathbb{H}_{\bar{e}}|}$ possibilities. For each subset $\delta\mathbb{H}_{\bar{e}} \subseteq \mathbb{H}_{\bar{e}}$, Alg. 3 explores $\binom{|\mathcal{D}|+|\delta\mathbb{H}_{\bar{e}}|-1}{|\delta\mathbb{H}_{\bar{e}}|}$ data-rate multi-sets. The number of permutations of a multiset $\mathbb{D}_{\delta\mathbb{H}_{\bar{e}}}$ of cardinality $|\delta\mathbb{H}_{\bar{e}}|$ is given by $\frac{|\delta\mathbb{H}_{\bar{e}}|!}{\Pi_{d_j \in \mathcal{D}} m_1(d_j)!}$ [59]. This results in $\frac{(|\mathcal{D}|+|\delta\mathbb{H}_{\bar{e}}|-1)!}{(|\mathcal{D}|-1)! \times \Pi_{d_j \in \mathcal{D}} m_1(d_j)!}$ enumerations. Then Alg. 3 enumerates $\mathcal{M}(\mathbb{P}_{\delta\mathbb{H}_{\bar{e}}})$ multi-sets of SPaths based on an SPath set $P_{\delta\mathbb{H}_{\bar{e}}}$, and this enumeration has an upper bound $\binom{q-1}{\frac{q}{2}} = \frac{\Pi_{j=\lceil \frac{q}{2} \rceil + 1}^{q-1} j!}{\lceil \frac{q}{2} \rceil !}$. Assuming that for each SPath $p \in P_{\delta\mathbb{H}_{\bar{e}}}$, Alg. 3 can have a data-rate multi-set $\mathbb{D}_p = (\mathcal{D}, m_3)$, where $m_3 : \mathcal{D} \rightarrow N$ is the frequency of a data-rate in $\mathbb{D}_p$, the number of data-rate permutations in $\mathcal{M}(\mathrm{D}_{\mathbb{P}_{\delta\mathbb{H}_{\bar{e}}}})$ is $\Pi_{i=1}^{|P_{\delta\mathbb{H}_{\bar{e}}}|} \frac{(|\mathcal{D}|+m_2(p_i)-1)!}{(|\mathcal{D}|-1)! \times \Pi_{d_j \in \mathcal{D}} m_3(d_j)!}$. Since MDP's time complexity is $\frac{q!}{\Pi_{p_j \in \mathbb{P}_{\delta\mathbb{H}_{\bar{e}}}} m_2(p_j)!}$ as per [52], the running time of Alg. 3 becomes $2^{|\mathbb{H}_{\bar{e}}|} \times \frac{(|\mathcal{D}|+|\delta\mathbb{H}_{\bar{e}}|-1)!}{(|\mathcal{D}|-1)! \times \Pi_{d_j \in \mathcal{D}} m_1(d_j)!} \times \frac{\Pi_{j=\lceil \frac{q}{2} \rceil + 1}^{q-1} j!}{\lceil \frac{q}{2} \rceil !} \times \Pi_{i=1}^{|P_{\delta\mathbb{H}_{\bar{e}}}|} \frac{(|\mathcal{D}|+m_2(p_i)-1)!}{(|\mathcal{D}|-1)! \times \Pi_{d_j \in \mathcal{D}} m_3(d_j)!} \times \frac{q!}{\Pi_{p_j \in \mathbb{P}_{\delta\mathbb{H}_{\bar{e}}}} m_2(p_j)!}$.

As Alg. 3 keeps the size of $\mathbb{H}_{\bar{e}}$ small, the running time is dominated by the latter part. However, typical values of $|\mathcal{D}|$ and q are small and we apply several pruning techniques to improve the running time.

Algorithm 3: Find the embedding of a single VLink

1 **function** *FindEmbedding*($G, \bar{e}, \mathcal{P}_{\bar{e}}^k, \mathcal{T}_{\bar{e}}, \sigma$)
2 **while** *A new* $H_{\bar{e}}$ *exists* **do**
3 Compute a new disjoint path group $H_{\bar{e}}$ using (13)
4 $\mathcal{H}_{\bar{e}} \leftarrow \mathcal{H}_{\bar{e}} \cup H_{\bar{e}}$
5 **for** $i = 2$ *to* $\max_{\forall H_{\bar{e}} \in \mathcal{H}_{\bar{e}}} |H_{\bar{e}}|$ **do**
6 $Z_{\bar{e}}^i \leftarrow \{H_{\bar{e}} | H_{\bar{e}} \in \mathcal{H}_{\bar{e}} \wedge |H_{\bar{e}}| = i\}$
7 $\mathcal{Z}_{\bar{e}}^i \leftarrow$ First σ $H_{\bar{e}} \in Z_{\bar{e}}^i$ with smallest avg. dist.
8 $\mathbb{H}_{\bar{e}} \leftarrow \mathbb{H}_{\bar{e}} \cup \mathcal{Z}_{\bar{e}}^i$
9 **foreach** $\delta\mathbb{H}_{\bar{e}} \subseteq \mathbb{H}_{\bar{e}}$ **do**
10 $\mathcal{M}(\mathbb{D}_{\delta\mathbb{H}_{\bar{e}}}) \leftarrow$ All-Multi-Set($\mathcal{D}, |\delta\mathbb{H}_{\bar{e}}|$) s.t. $\sum_{d \in \mathbb{D}_{\delta\mathbb{H}_{\bar{e}}}} d = \bar{\beta}_{\bar{e}}$
11 **foreach** $\mathbb{D}_{\delta\mathbb{H}_{\bar{e}}} \in \mathcal{M}(\mathbb{D}_{\delta\mathbb{H}_{\bar{e}}})$ **do**
12 $\zeta(\mathbb{D}_{\delta\mathbb{H}_{\bar{e}}}) \leftarrow$ All-Permutation($\mathbb{D}_{\delta\mathbb{H}_{\bar{e}}}$)
13 **foreach** $\mathrm{D}_{\delta\mathbb{H}_{\bar{e}}} \in \zeta(\mathbb{D}_{\delta\mathbb{H}_{\bar{e}}})$ **do**
14 **foreach** $H_{\bar{e}} \in \delta\mathbb{H}_{\bar{e}}$ **do**
15 $d_{H_{\bar{e}}} \leftarrow \mathrm{D}_{\delta\mathbb{H}_{\bar{e}}}$[index of $H_{\bar{e}} \in \delta\mathbb{H}_{\bar{e}}$]
16 Compute $d_{p_{H_{\bar{e}}}}$ using (14)
17 Compute $d_{p_{\delta\mathbb{H}_{\bar{e}}}}$ using (15)
18 $\mathcal{M}(\mathbb{P}_{\delta\mathbb{H}_{\bar{e}}}) \leftarrow$ All-Multi-Set($P_{\delta\mathbb{H}_{\bar{e}}}, q$)
19 **foreach** $\mathbb{P}_{\delta\mathbb{H}_{\bar{e}}} \in \mathcal{M}(\mathbb{P}_{\delta\mathbb{H}_{\bar{e}}})$ **do**
20 **foreach** $p \in \mathbb{P}_{\delta\mathbb{H}_{\bar{e}}}$ **do**
21 $\mathcal{M}(\mathbb{D}_p) \leftarrow$ All-Multi-Set($\mathcal{D}, m_2(p)$) s.t. $\sum_{d \in \mathbb{D}_p} d = d_{p_{\delta\mathbb{H}_{\bar{e}}}}$
22 **foreach** $\mathbb{D}_p \in \mathcal{M}(\mathbb{D}_p)$ **do**
23 $\zeta(\mathbb{D}_p) \leftarrow$ All-Permutation($\mathbb{D}_p$)
24 $\mathcal{M}(\mathrm{D}_{\mathbb{P}_{\delta\mathbb{H}_{\bar{e}}}}) \leftarrow \zeta(\mathbb{D}_{p_1}) \times \zeta(\mathbb{D}_{p_2}) ... \times \zeta(\mathbb{D}_{p_{|P_{\delta\mathbb{H}_{\bar{e}}}|}})$
  foreach $\mathrm{D}_{\mathbb{P}_{\delta\mathbb{H}_{\bar{e}}}} \in \mathcal{M}(\mathrm{D}_{\mathbb{P}_{\delta\mathbb{H}_{\bar{e}}}})$ **do**
25 $< n, \mathbb{P}, \mathbb{T}, \mathbb{S} > \leftarrow$ MDP($\mathbb{P}_{\delta\mathbb{H}_{\bar{e}}}, \mathrm{D}_{\mathbb{P}_{\delta\mathbb{H}_{\bar{e}}}}$)
26 Find $\mathbb{P}^{opt}$, $\mathbb{T}^{opt}$ and $\mathbb{S}^{opt}$ that minimizes (8)
27 $\mathcal{I}_{\bar{e}} \leftarrow < \mathbb{P}^{opt}, \mathbb{T}^{opt}, \mathbb{S}^{opt} >$
28 **return** $\mathcal{I}_{\bar{e}}$

VI. Evaluation

We evaluate the proposed solutions through extensive simulations. Section VI-A describes the simulation setup in detail and Section VI-B defines the performance metrics. Then we present our evaluation results focusing on the following three aspects. First, we perform micro-benchmarks of our solutions and compare with the demand splitting model presented in [45]), a recent work on survivable VNE over flexible grid optical networks. For the micro-benchmark scenario, we consider each VN embedding request in isolation and assume that the VN can always be embedded on the EON. Under these assumptions, we measure the resource efficiency of our

proposed solutions. Second, we analyze the performance of the heuristic algorithm in both small and large scale settings considering each VN embedding request in isolation. Finally, we perform steady state analysis of our heuristic solution. The steady state analysis considers VN arrivals and departures over a period of time and also considers the possibility of failing to embed a VN request on the EON. The steady state analysis provides valuable insights into the number of accepted VNs and the EON link utilization in a longer time frame.

A. Simulation Setup

1) Testbed: We implement the ILP formulation from Section IV using IBM ILOG CPLEX C++ libraries. We compare the ILP's solution with a C++ implementation of the heuristic presented in Section V. Simulations are run on a machine with 8×10-core Intel Xeon E7-8870 2.40GHz processors and 1TB RAM. We developed a discrete event simulator that simulates the arrival and departure of VNs for the steady state scenario.

2) SN characteristic: We use Nobel Germany (17 nodes and 26 links) and Germany50 (50 nodes and 88 links) networks from SNDlib repository [60] as the EONs for small and large scale simulations, respectively. We pre-compute $k = 25$ and $k = 20$ shortest paths between all pairs of SNodes as inputs to our simulation for Nobel Germany and Germany50 SN, respectively. Each SLink in the EON has spectrum bandwidth of 600GHz and 4THz for small and large scale simulations, respectively [61]. We also vary the Link-to-Node Ratio (LNR) of Nobel Germany SN by adding or removing some links in the original topology (original LNR is 1.53). This is done to show the impact of different levels of SN densities on the performance metrics. For steady state analysis, we use Nobel Germany topology as the EON and set 4THz spectrum bandwidth on each SLink.

3) VN generation: We synthetically generate VNs with different properties. For the small-scale scenario, we restrict VN sizes to 4 VNodes and 5 VLinks to limit the ILP's complexity. For the large-scale scenario, we generate VNs with 20 VNodes and 30 VLinks. We set VLink demands to multiples of 100Gbps, ranging between 100Gbps and 1Tbps, following the granularity of commercial transponders. Node mapping of VNodes to SNodes is randomly chosen. In our simulations, we vary BSR from 0% to 100% with 20%-point increments. Here, $BSR = 0$ means no protection and $BSR = 100\%$ provides full dedicated protection. We generate 5 and 20 different VNs with similar total bandwidth demands for small- and large-scale simulations, respectively, and take the mean of the performance metrics over those VNs.

For the steady state analysis, we simulate VN arrival and departure scenarios with different arrival rates. The VN arrival rate of each scenario follows a Poisson distribution. We vary the mean of the Poisson distribution between 4 – 12 VNs per 100 time units. VN life time in all the scenarios is exponentially distributed with a mean of 100 time units. We generate each arrived VN with random connectivity between VNodes. We keep the number of VNodes of each arrived VN at 4, and chose the LNR of the VN randomly between 1 and 3.5. VLink demands are chosen in the same way as in the micro-benchmark scenario.

To demonstrate the impact of different BSR requirements on the blocking ratio and at the same time to simulate the behavior of different VN characteristics and requirements, we generate BSR of each VN using a Binomial distribution. For each arrival rate, we generate 5 simulation scenarios, each with a different Binomial distribution of BSRs. For these 5 scenarios, we set the mean of the Binomial distribution to 0, 20, 40, 60, and 80%-points, respectively. We run the simulation for 10000 simulated time units and exclude measurements from the first 1000 time units to capture the steady state performance. For each problem instance with a fixed arrival rate and mean BSR, we generate 5 random simulation scenarios and report the mean performance metrics to gain statistical confidence. These parameters have been chosen in accordance with those used in the network virtualization literature (*e.g.*, [57], [62], [63]).

B. Compared Variants

In our evaluation, we quantify the impact of the two key flexibilities introduced by EONs, namely, adaptability in transponder configuration (*i.e.*, variable FEC and modulation) and in spectrum allocation. In doing so, we compare the variants listed in Table II. *Fix-RT* considers fixed-grid spectrum allocation with only one tuple for modulation format, FEC overhead, and reach for each fixed-grid data rate in $\mathcal{R}$ and serves as the baseline for our evaluation. In contrast, the other two variants, *Fix-AT* and *Flex-AT*, exploit a transponder's capability to choose from a variety of modulation formats and/or FEC overheads for each data rate in $\mathcal{R}$, leading to different reaches. These two variants differ in terms of spectrum slot allocation granularity (*i.e.*, 50GHz and 12.5GHz for fixed-grid and flex-grid, respectively) and the total number of possible data rates (*i.e.*, 100G, 200G, 400G for fixed-grid and 100G, 150G, 200G, 250G, 300G, 400G, 500G, 600G, and 800G for flex-grid). Spectrum occupation and data rates of each variant are chosen based on current industry standards [61]. We set $q = 8$ to keep the number of used transponders reasonable.

TABLE II
COMPARED VARIANTS

Variant	Transponder Flexibility	Flexible Spectrum Allocation
Fix-RT	No	No
Fix-AT	Yes	No
Flex-AT	Yes	Yes

C. Performance Metrics

a) Spectrum slot Usage (SSU): The total number of spectrum slots required to embed a VN. This metric is computed using only the first term of (8).

b) Protection overhead: Ratio between total bandwidth allocated of a VLink (on all different splits) and the actual bandwidth demand of the VLink. It is a measure of the required extra bandwidth for providing protection.

c) Max. no. of disjoint paths: Average of the maximum number of disjoint SPaths used to embed a VLink.

d) Max. no. of splits: Average of the maximum number of splits used to embed a VLink.

This article has been accepted for publication in a future issue of this journal, but has not been fully edited. Content may change prior to final publication. Citation information: DOI 10.1109/TNSM.2020.2992442, IEEE Transactions on Network and Service Management

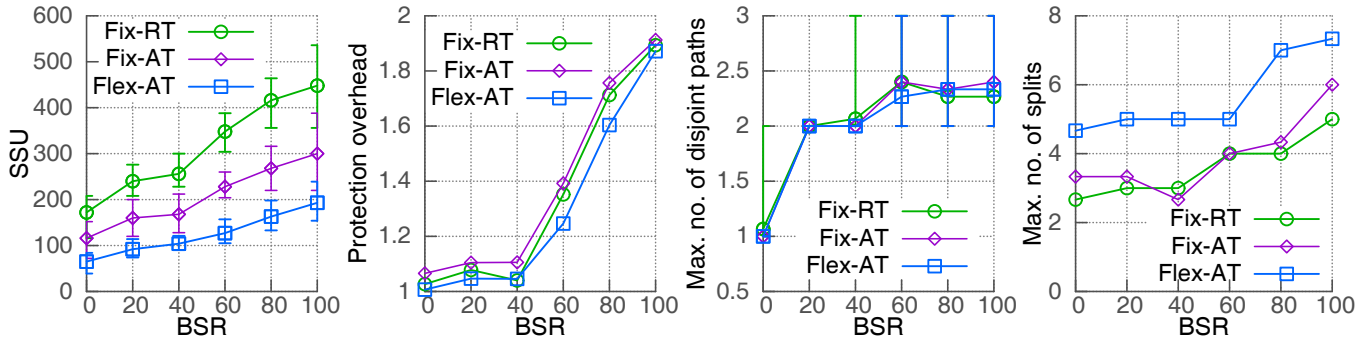

(a) Impact on SSU (b) Impact on protection overhead (c) Impact on number of disjoint paths (d) Impact on number of splits

Fig. 4. Impact of varying BSR on performance metrics in Nobel Germany EON

e) Cost ratio: The ratio of costs obtained by two different approaches for solving the same problem instance, where cost is computed using (8).

f) Execution time: The time required for an algorithm to find a VN embedding.

g) Blocking ratio: The fraction of VN requests that could not be embedded on the EON over all the VN requests in a simulation.

h) Link utilization: The ratio between the number of slots used in an SLink and the total number of slots in the SLink at any instance of time.

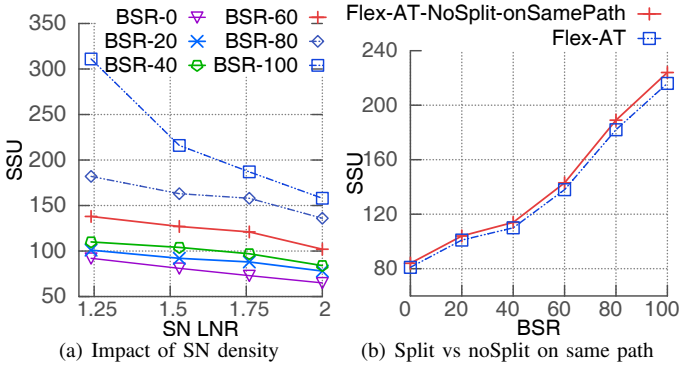

(a) Impact of SN density (b) Split vs noSplit on same path

Fig. 5. Analysis of our reliability model using the Nobel Germany EON

D. Micro-benchmark results

1) Small-scale results with ILP formulation: Fig. 4 presents the impact of varying BSR on all performance metrics, and for all the compared variants, in Nobel Germany SN. Specifically, Fig. 4(a) shows that SSU is the highest for the baseline variant, *Fix-RT*, since it does not allow any flexibility in tuning transmission parameters or spectrum allocation. In contrast, *Fix-AT* uses 30% less spectrum resources on average compared to *Fix-RT* by only using tunable transponders with coarse-grained spectrum allocation. By combining flexible spectrum allocation with transponder tunability, *Flex-AT* saves on average 57% and 27% spectrum compared to *Fix-RT* and *Fix-AT*, respectively. Lastly, *Fix-RT* was infeasible for some problem instances at BSR > 80 due to its inflexibility in transmission configuration tuning and spectrum allocation.

Fig. 4(a) also shows that SSU increases for increasing BSR in all considered cases. However, SSU rises very slowly (remaining within 10% of the originally requested bandwidth). 10% additional bandwidth is due to the lack of fine-grained data rates that results in a small amount of over-provisioning (*e.g.*, 350Gbps is needed for BSR=40% and demand=800Gbps, as 320Gbps is not a valid data rate). when BSR $\leq 40\%$, while it steeply increases for BSR $> 40\%$. This can be explained by observing how the protection overhead (see plot in Fig. 4(b)) behaves for BSR up to 40%. This behavior of the protection overhead for BSR $\leq 40\%$ confirms the intuition, already discussed in Section I, that low BSR can be guaranteed with low or no additional bandwidth if at least two disjoint SPaths can be used to map the splits of a VLink. In contrast, for BSR $> 40\%$, more than two disjoint SPaths are needed for each VLink to reduce protection overhead. However, in our SN (Nobel Germany), either more than two disjoint SPaths do not exist for some pairs of SNodes, or the third and higher order disjoint SPaths become too long due to the sparse connectivity of the SN. Since long SPaths can support only low modulation formats, and thus require high number of spectrum slots, they are very unlikely to be selected in the optimal solution. This can be verified in Fig. 4(c), where it can be seen that the max. no. of disjoint SPaths used to embed a VLink is slightly larger than two for BSR $> 40\%$, thus increasing protection overhead and, eventually, SSU.

Fig. 4(d) shows that the max. no. of splits of a VLink is always larger than the max. no. of disjoint SPaths of a VLink, implying that there are multiple splits on the same SPath. Note also that Fig. 4(d) shows that *Flex-AT* uses the highest number of splits to minimize the SSU as shown in Fig. 4(a). This is due to *Flex-AT*'s smaller granularity in spectrum allocation that allows to use shorter SPaths even if the spectrum resources on these SPaths are fragmented.

To demonstrate how SN connectivity impacts spectral efficiency, Fig. 5(a) shows SSU for *Flex-AT* with different BSR requirements by varying LNR of Nobel Germany SN. Fig. 5 shows that SSUs decrease with increasing SN LNR even for the no protection case (0% BSR). This stems from the fact that an SN with a larger LNR reduces the lengths and the number of intermediate hops of the SPaths between the same pair of SNodes, thus facilitating the use of more spectrum efficient transmission configurations along fewer hops. However, the gain in spectrum saving by increasing SN LNR is much higher for high BSR requirements. The additional gain is due to the

This article has been accepted for publication in a future issue of this journal, but has not been fully edited. Content may change prior to final publication. Citation information: DOI 10.1109/TNSM.2020.2992442, IEEE Transactions on Network and Service Management

use of three or more disjoint SPaths for mapping a VLink, thanks to the higher path diversity of a densely connected SN.

Finally, Fig. 5(b) demonstrates the benefit of our splitting model that enables *Flex-AT* to save 3%–4% SSU compared to a case in which splitting is allowed over different SPaths, but not over the same SPath on different spectrum segments (*Flex-AT-NoSplit-onSamePath*, e.g., the splitting model of [45]). Note that *NoSplit-onSamePath* model renders problem instances with high BSR in *Fix-RT* and *Fix-AT* cases infeasible as spectrum fragmentation prohibits only one split per feasible SPath to occupy the required spectrum. In contrast, our model finds solutions in those cases by increasing number of splits per SPath even in fragmented situations as shown in Fig. 4(a) and Fig. 4(d). It is worth noting that our splitting model does not require any additional hardware investment, so the savings ($\sim 4\%$) by our splitting model shown in Fig. 5(b) are achieved at no additional cost.

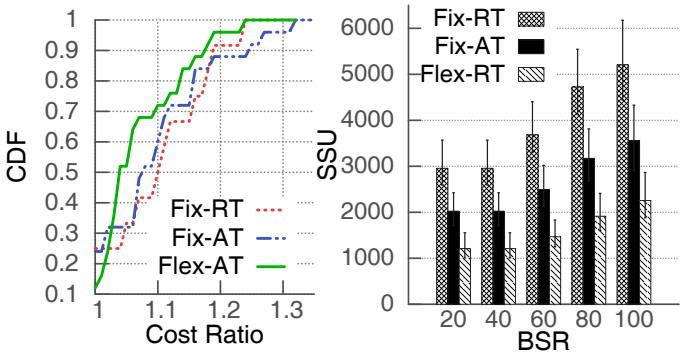

(a) Cost ratio (Nobel Germany EON) (b) SSU (Germany50 EON)

Fig. 6. Performance of our Heuristic Algorithm

2) Performance of the Heuristic Algorithm: As our cost function (8) is dominated by SSU, the cost ratio between heuristic and ILP gives a measure of how much additional resources are allocated by the heuristic. We present the cumulative distribution function (CDF) of cost ratios in Fig. 6(a). Over all, the heuristic incurs 12%, 9%, and 7% additional cost on average compared to the ILP for *Fix-RT*, *Fix-AT*, and *Flex-AT*, respectively, while executing 2 or 3 orders of magnitude faster. Fig. 6(b) shows SSU incurred by the heuristic algorithm in Germany50 SN. Fig. 6(b) confirms the conclusions observed in Fig. 4, but with much larger and higher number of VNs, a bigger SN, and full 4THz spectrum resources on SLinks and by repeating our simulations over a much higher number of instances to achieve statistical confidence.

3) Scalability of the heuristic: We demonstrate the scalability of our heuristic algorithm compared to that of the ILP-based optimal solution by comparing their execution time in Fig. 7. Fig. 7(a) shows the execution times of the ILP and heuristic algorithm on the small scale scenario. When we consider flex-grid spectrum allocation and flexible transponders, the ILP can take several hours to embed a VN with dedicated backup resources. With the increase in BSR, the solution space becomes larger hence the increase in execution time for ILP-Flex-AT. Compared to the ILP based solutions, the heuristic finds a solution several orders of magnitude faster. For the large scale scenario, the heuristic is able to find solutions

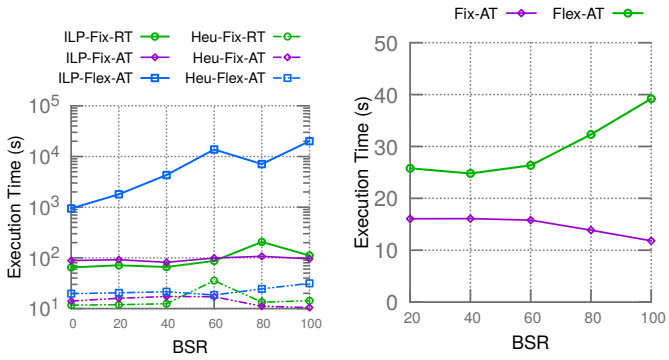

(a) Small Scale (Nobel Germany) (b) Large Scale (Germany50)

Fig. 7. Execution Time

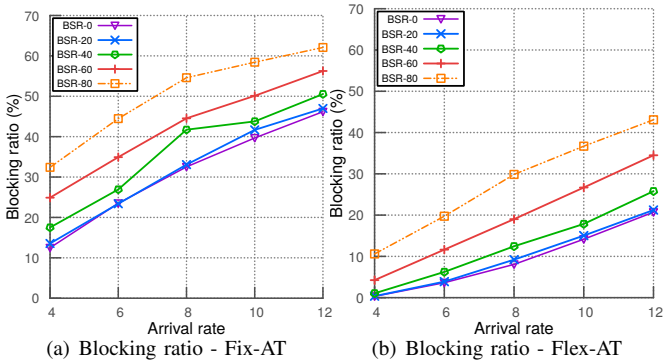

(a) Blocking ratio - Fix-AT (b) Blocking ratio - Flex-AT

Fig. 8. Blocking ratio (Nobel Germany EON)

in less than a minute (Fig. 7(b)) for the largest VN in our simulation. Again there is an increasing trend in execution time with increasing BSR for Flex-AT due to larger solution space. In contrast, the ILP fails to solve even a single problem instance in large scale scenario, limiting its scalability to only small scale problem instances.

E. Steady state analysis

1) Blocking Ratio: Fig. 8 presents average blocking ratio for increasing arrival rate and different BSR considering both fixed- (Fig. 8(a)) and flex-grid (Fig. 8(b)) spectrum allocation using flexible transponders. The results on blocking ratio reaffirms our previous finding that BSR less than 40% incurs very little protection overhead for the VNs. As a result, we see nearly identical blocking ratio for BSR 20% and BSR 0% (*i.e.*, no protection baseline scenario) in case of both fixed- and flex-grid EONs. Indeed, flex-grid EON has finer-grained resource allocation capabilities, resulting in significantly less blocking ratio for the same load levels compared to fixed-grid spectrum allocation. With increasing BSR, especially beyond BSR 40%, the protection overhead significantly increases for the same VN request, hence, the increasing gap between different BSRs in Fig. 8(a) and Fig. 8(b).

2) Substrate Link Utilization: Fig. 9 presents the average utilization of the substrate links during the course of simulation with 5th and 95th percentile errorbars. For a given load, *i.e.*, arrival rate, we see that link utilization does not significantly vary across different BSRs. From the first look, this result is

This article has been accepted for publication in a future issue of this journal, but has not been fully edited. Content may change prior to final publication. Citation information: DOI 10.1109/TNSM.2020.2992442, IEEE Transactions on Network and Service Management

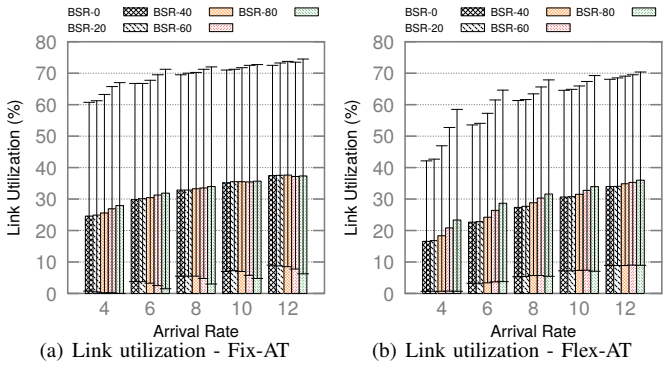

(a) Link utilization - Fix-AT (b) Link utilization - Flex-AT

Fig. 9. Substrate Link Utilization (Nobel Germany EON)

counter-intuitive and does not seem to agree with the result from Fig. 8. One would expect a high blocking ratio resulting from the substrate links becoming saturated. In other words, link utilization for BSR 80% was expected to be significantly higher compared to BSR 0%. However, even though a higher BSR results in lesser number of admitted VNs, it also results in higher protection overhead for the embedded VNs. As a consequence, for the same arrival rate with different BSR requirements, the higher BSR requirement will end up using more number of spectrum slots in the substrate links. This results in similar level of spectrum occupancy even with lower number of VNs admitted due to higher BSR requirement.

VII. Conclusion

This paper addresses a fundamental problem for the slicing of 5G transport networks, *i.e.*, reliable VN embedding with dedicated protection in an EON. To reduce resource overbuild of dedicated protection, we exploit bandwidth squeezing and VLink demand splitting over multiple SPaths, while leveraging the flexibility offered by an EON. Our novel splitting model not only provides the opportunity to split a VLink demand across multiple SPaths but also across multiple spectrum segments of an SPath. We present an ILP formulation to solve the problem optimally, and a heuristic solution to address the computational complexity of the ILP. Our simulations on realistic network topologies show that bandwidth squeezing and demand splitting allow to significantly reduce spectrum usage for providing dedicated protection, especially in the case of fully-flexible EON. Our evaluation also shows that the opportunity to have multiple splits over the same path allows to save additional spectrum compared to a model that does not allow splitting on the same path, and our proposed heuristic performs close to the optimal solution. For instance, multiple splits enable us to guarantee a BSR 40% with only 10% additional spectrum resources. This translates into similar VN blocking ratio up to 40% BSR. Our discrete event simulation also shows that similar spectrum occupancy is achieved on EON links irrespective of BSR requirement for a given VN arrival rate. However, spectrum occupancy increases with the increase in VN arrival rate.

We hope that these promising results will further stimulate research in achieving reliable slicing of a fully flexible 5G transport EON. Interesting research directions include recovery of VNs after permanent substrate link failures and EON node failures and re-optimization of VN embedding by leveraging EON flexibility. Another interesting research direction is to investigate how physical layer demand split information can be leveraged at the transport and application layer for taking better flow scheduling decisions.

References

[1] N. Shahriar, S. Taeb, S. R. Chowdhury, M. Zulfiqar, M. Tornatore, R. Boutaba, J. Mitra, and M. Hemmati, "Reliable slicing of 5G transport networks with dedicated protection," in *Proc. of IEEE/ACM CNSM*, 2019, pp. 1–9.

[2] S. Gringeri, B. Basch, V. Shukla, R. Egorov, and T. J. Xia, "Flexible architectures for optical transport nodes and networks," *IEEE Commun. Mag.*, vol. 48, no. 7, pp. 40–50, 2010.

[3] S. Aleksic, "Towards fifth-generation (5G) optical transport networks," in *Proc. of ICTON*, 2015, pp. 1–4.

[4] R. Boutaba, N. Shahriar, and S. Fathi, "Elastic optical networking for 5G transport," *Journal of Netw. and Syst. Man.*, vol. 25, no. 4, pp. 819–847, 2017.

[5] X. Foukas, G. Patounas, A. Elmokashfi, and M. K. Marina, "Network slicing in 5G: Survey and challenges," *IEEE Commun. Mag.*, vol. 55, no. 5, pp. 94–100, 2017.

[6] M. Hadi, M. R. Pakravan, and E. Agrell, "Dynamic resource allocation in metro elastic optical networks using lyapunov drift optimization," *Journal of Opt. Commun. & Netw.*, vol. 11, no. 6, pp. 250–259, 2019.

[7] B. M. Khorsandi, F. Tonini, E. Amato, and C. Raffaelli, "Dedicated path protection for reliable network slice embedding based on functional splitting," in *Proc. of IEEE ICTON*, 2019, pp. 1–4.

[8] "Meeting 5G transport requirements with FlexE," White paper, ZTE, 2018.

[9] R. Roy and B. Mukherjee, "Degraded-service-aware multipath provisioning in telecom mesh networks," in *Proc. of IEEE/OSA OFC*, 2008.

[10] Y. Sone, A. Watanabe, W. Imajuku, Y. Tsukishima, B. Kozicki, H. Takara, and M. Jinno, "Bandwidth squeezed restoration in spectrum-sliced elastic optical path networks (slice)," *IEEE/OSA Journal of Opt. Commun. and Netw.*, vol. 3, no. 3, pp. 223–233, 2011.

[11] X. Chen, M. Tornatore, S. Zhu, F. Ji, W. Zhou, C. Chen, D. Hu, L. Jiang, and Z. Zhu, "Flexible availability-aware differentiated protection in software-defined elastic optical networks," *IEEE/OSA Journal of Lightwave Tech.*, vol. 33, no. 18, pp. 3872–3882, 2015.

[12] K. D. R. Assis, S. Peng, R. C. Almeida, H. Waldman, A. Hammad, A. F. Santos, and D. Simeonidou, "Network virtualization over elastic optical networks with different protection schemes," *IEEE/OSA Journal of Opt. Commun. and Netw.*, vol. 8, no. 4, pp. 272–281, Apr 2016.

[13] S. Huang, C. U. Martel, and B. Mukherjee, "Survivable multipath provisioning with differential delay constraint in telecom mesh networks," *IEEE/ACM Trans. on Netw.*, vol. 19, no. 3, pp. 657–669, Jun. 2011.

[14] M. M. A. Khan, N. Shahriar, R. Ahmed, and R. Boutaba, "SiMPLE: Survivability in multi-path link embedding," in *Proc. of IEEE/ACM CNSM*, 2015, pp. 210–218.

[15] A. Markopoulou, G. Iannaccone, S. Bhattacharyya, C.-N. Chuah, and C. Diot, "Characterization of failures in an ip backbone," in *Proceedings of IEEE INFOCOM 2004*, vol. 4, 2004, pp. 2307–2317.

[16] M. R. Rahman, I. Aib, and R. Boutaba, "Survivable virtual network embedding," in *Proceedings of IFIP Networking*, 2010, pp. 40–52.

[17] S. Ramamurthy, L. Sahasrabuddhe, and B. Mukherjee, "Survivable wdm mesh networks," *IEEE/OSA Journal of Lightwave Tech.*, vol. 21, no. 4, p. 870, 2003.

[18] Z. Ye, A. N. Patel, P. N. Ji, and C. Qiao, "Survivable virtual infrastructure mapping with dedicated protection in transport software-defined networks," *IEEE/OSA Journal of Opt. Commun. and Netw.*, vol. 7, no. 2, pp. A183–A189, 2015.

[19] S. R. Chowdhury, R. Ahmed, M. M. A. Khan, N. Shahriar, R. Boutaba, J. Mitra, and F. Zeng, "Protecting virtual networks with drone," *IEEE Trans. on Netw. and Serv. Man.*, vol. 13, pp. 913–926, 2016.

[20] N. Shahriar, S. R. Chowdhury, R. Ahmed, A. Khan, S. Fathi, R. Boutaba, J. Mitra, and L. Liu, "Virtual network survivability through joint spare capacity allocation and embedding," *IEEE Journal on Selected Areas in Commun.*, vol. 36, no. 3, pp. 502–518, 2018.

[21] T. Guo, N. Wang, K. Moessner, and R. Tafazolli, "Shared backup network provision for virtual network embedding," in *Proc. of IEEE ICC*, 2011, pp. 1–5.

[22] N. Shahriar, R. Ahmed, A. Khan, S. R. Chowdhury, R. Boutaba, and J. Mitra, "ReNoVatE: Recovery from node failure in virtual network embedding," in *Proc. of IEEE/ACM CNSM*, 2016, pp. 19–27.
[23] A. Castro, L. Velasco, M. Ruiz, and J. Comellas, "Single-path provisioning with multi-path recovery in flexgrid optical networks," in *Proc. of UMTCS*, 2012, pp. 745–751.
[24] M. Liu, M. Tornatore, and B. Mukherjee, "Survivable traffic grooming in elastic optical networks—shared protection," *Journal of Lightwave Tech.*, vol. 31, no. 6, pp. 903–909, 2013.
[25] G. Shen, Y. Wei, and S. Bose, "Optimal design for shared backup path protected elastic optical networks under single-link failure," *IEEE/OSA Journal of Opt. Commun. and Netw.*, vol. 6, no. 7, pp. 649–659, 2014.
[26] H. Yang, X. Zhu, W. Bai, Y. Zhao, J. Zhang, Z. Liu, Z. Zhou, and Q. Ou, "Survivable von mapping with ambiguity similitude for differentiable maximum shared capacity in elastic optical networks," *Optical Fiber Technology*, vol. 31, pp. 138–146, 2016.
[27] Y. Wang, X. Li, B. Guo, T. Gao, W. Li, and S. Huang, "Survivable virtual optical network mapping in elastic optical networks with shared backup path protection," in *Proc. of WOCC*, 2016, pp. 1–4.
[28] A. Cai, J. Guo, R. Lin, G. Shen, and M. Zukerman, "Multicast routing and distance-adaptive spectrum allocation in elastic optical networks with shared protection," *IEEE/OSA Journal of Lightwave Tech.*, vol. 34, no. 17, pp. 4076–4088, 2016.
[29] C. Wang, G. Shen, and S. K. Bose, "Distance adaptive dynamic routing and spectrum allocation in elastic optical networks with shared backup path protection," *IEEE/OSA Journal of Lightwave Technology*, vol. 33, no. 14, pp. 2955–2964, 2015.
[30] S. Yin, S. Huang, B. Guo, Y. Zhou, H. Huang, M. Zhang, Y. Zhao, J. Zhang, and W. Gu, "Shared-protection survivable multipath scheme in flexible-grid optical networks against multiple failures," *IEEE/OSA Journal of Lightwave Tech.*, vol. 35, no. 2, pp. 201–211, 2016.
[31] C. Ou, L. H. Sahasrabuddhe, K. Zhu, C. U. Martel, and B. Mukherjee, "Survivable virtual concatenation for data over sonet/sdh in optical transport networks," *IEEE/ACM Trans. on Netw.*, vol. 14, no. 1, pp. 218–231, 2006.
[32] O. Hauser, M. Kodialam, and T. Lakshman, "Capacity design of fast path restorable optical networks," in *Proc. of IEEE INFOCOM*, 2002, pp. 817–826.
[33] W. Wang, Y. Lin, Y. Zhao, G. Zhang, J. Zhang, J. Han, H. Chen, B. Hou, Y. Ji, and L. Zong, "First demonstration of virtual transport network services with multi-layer protection schemes over flexi-grid optical networks," *IEEE Com. Letters*, vol. 20, no. 2, pp. 260–263, 2015.
[34] H. Jiang, L. Gong, and Z. Zuqing, "Efficient joint approaches for location-constrained survivable virtual network embedding," in *Proc. of IEEE GLOBECOM*, 2014, pp. 1810–1815.
[35] M. Klinkowski, "A genetic algorithm for solving rsa problem in elastic optical networks with dedicated path protection," in *Proceedings of International Joint Conference CISIS'12-ICEUTE´ 12-SOCO´ 12 Special Sessions*, 2013, pp. 167–176.
[36] M. Klinkowski, "An evolutionary algorithm approach for dedicated path protection problem in elastic optical networks," *Cybernetics and Systems*, vol. 44, no. 6-7, pp. 589–605, 2013.
[37] K. Walkowiak, M. Klinkowski, B. Rabiega, and R. Goścień, "Routing and spectrum allocation algorithms for elastic optical networks with dedicated path protection," *Elsevier Opt. Switching and Netw.*, vol. 13, pp. 63–75, 2014.
[38] W. Xie, J. P. Jue, Q. Zhang, X. Wang, Q. She, P. Palacharla, and M. Sekiya, "Survivable impairment-constrained virtual optical network mapping in flexible-grid optical networks," *IEEE/OSA Journal of Opt. Commun. and Netw.*, vol. 6, no. 11, pp. 1008–1017, 2014.
[39] B. Chen, J. Zhang, W. Xie, J. P. Jue, Y. Zhao, and G. Shen, "Cost-effective survivable virtual optical network mapping in flexible bandwidth optical networks," *IEEE/OSA Journal of Lightwave Tech.*, vol. 34, no. 10, pp. 2398–2412, 2016.
[40] Y. Zhao, B. Chen, J. Zhang, and X. Wang, "Energy efficiency with sliceable multi-flow transponders and elastic regenerators in survivable virtual optical networks," *IEEE Trans. on Commun.*, vol. 64, no. 6, pp. 2539–2550, 2016.
[41] Y. Kishi, N. Kitsuwan, H. Ito, B. C. Chatterjee, and E. Oki, "Modulation-adaptive link-disjoint path selection model for 1+ 1 protected elastic optical networks," *IEEE Access*, vol. 7, pp. 25 422–25 437, 2019.
[42] Y. Wei, K. Xu, H. Zhao, and G. Shen, "Applying p-cycle technique to elastic optical networks," in *Proc. of ONDM*, 2014, pp. 1–6.
[43] F. Ji, X. Chen, W. Lu, J. J. Rodrigues, and Z. Zhu, "Dynamic p-cycle protection in spectrum-sliced elastic optical networks," *IEEE/OSA Journal of Lightwave Tech.*, vol. 32, no. 6, pp. 1190–1199, 2014.
[44] X. Chen, F. Ji, and Z. Zhu, "Service availability oriented p-cycle protection design in elastic optical networks," *IEEE/OSA Journal of Opt. Commun. and Netw.*, vol. 6, no. 10, pp. 901–910, 2014.
[45] R. Goścień, K. Walkowiak, and M. Tornatore, "Survivable multipath routing of anycast and unicast traffic in elastic optical networks," *IEEE/OSA Journal of Opt. Commun. and Netw.*, vol. 8, no. 6, pp. 343–355, 2016.
[46] L. Ruan and N. Xiao, "Survivable multipath routing and spectrum allocation in OFDM-based flexible optical networks," *IEEE/OSA Journal of Opt. Commun. and Netw.*, vol. 5, no. 3, pp. 172–182, 2013.
[47] L. Ruan and Y. Zheng, "Dynamic survivable multipath routing and spectrum allocation in ofdm-based flexible optical networks," *Journal of Opt. Commun. and Netw.*, vol. 6, no. 1, pp. 77–85, 2014.
[48] A. Castro, L. Velasco, J. Comellas, and G. Junyent, "On the benefits of multi-path recovery in flexgrid optical networks," *Photonic Netw. Commun.*, vol. 28, no. 3, pp. 251–263, 2014.
[49] N. Amaya, G. Zervas, and D. Simeonidou, "Introducing node architecture flexibility for elastic optical networks," *IEEE/OSA Journal of Opt. Commun. and Netw.*, vol. 5, no. 6, pp. 593–608, 2013.
[50] G. Zhang, M. De Leenheer, A. Morea, and B. Mukherjee, "A survey on OFDM-based elastic core optical networking," *IEEE Commun. Surveys Tuts.*, vol. 15, no. 1, pp. 65–87, 2012.
[51] A. Pagès, J. Perelló, S. Spadaro, and J. Comellas, "Optimal route, spectrum, and modulation level assignment in split-spectrum-enabled dynamic elastic optical networks," *IEEE/OSA Journal of Opt. Commun. and Netw.*, vol. 6, no. 2, pp. 114–126, 2014.
[52] N. Shahriar, S. Taeb, S. R. Chowdhury, M. Tornatore, R. Boutaba, J. Mitra, and M. Hemmati, "Achieving a fully-flexible virtual network embedding in elastic optical networks," in *Proc. of IEEE INFOCOM*, 2019, pp. 1756–1764.
[53] G. Bernstein, D. Caviglia, R. Rabbat, and H. Van Helvoort, "Vcat-lcas in a clamshell," *IEEE Commun. Mag.*, vol. 44, no. 5, pp. 34–36, 2006.
[54] "Optical internetworking forum - flex ethernet implementation agreement 1.1," June 2017. [Online]. Available: https://www.oiforum.com/wp-content/uploads/2019/01/FLEXE1.1.pdf
[55] S. Taeb, N. Shahriar, S. R. Chowdhury, M. Tornatore, R. Boutaba, J. Mitra, and M. Hemmati, "Virtual network embedding with path-based latency guarantees in elastic optical networks," in *Proc. of IEEE ICNP*, 2019, pp. 1–12.
[56] Y. Wang, X. Cao, and Y. Pan, "A study of the routing and spectrum allocation in spectrum-sliced elastic optical path networks," in *Proc. of IEEE INFOCOM*, 2011, pp. 1503–1511.
[57] M. Chowdhury, M. R. Rahman, and R. Boutaba, "Vineyard: Virtual network embedding algorithms with coordinated node and link mapping," *IEEE/ACM Trans. on Netw.*, vol. 20, no. 1, pp. 206–219, 2012.
[58] B. C. Chatterjee, N. Sarma, and E. Oki, "Routing and spectrum allocation in elastic optical networks: A tutorial," *IEEE Communications Surveys & Tutorials*, vol. 17, no. 3, pp. 1776–1800, 2015.
[59] R. A. Brualdi, "Introductory combinatorics," *New York*, vol. 3, 1992.
[60] Sndlib repository [online] http://sndlib.zib.de/home.action.
[61] ITU-T G.694.1. spectral grids for WDM applications: DWDM frequency grid.[online] https://www.itu.int/rec/t-rec-g.694.1/en.
[62] S. R. Chowdhury, S. Ayoubi, R. Ahmed, N. Shahriar, R. Boutaba, J. Mitra, and L. Liu, "Multi-layer virtual network embedding," *IEEE Trans. on Netw. and Serv. Man.*, vol. 15, no. 3, pp. 1132–1145, 2018.
[63] N. Shahriar, R. Ahmed, S. R. Chowdhury, M. M. A. Khan, R. Boutaba, J. Mitra, and F. Zeng, "Virtual network embedding with guaranteed connectivity under multiple substrate link failures," *IEEE Trans. on Commun.*, vol. 68, no. 2, pp. 1025–1043, 2020.

Nashid Shahriar (S'16) is a Ph.D. candidate at the School of Computer Science, University of Waterloo. He received M.Sc. and B.Sc. degrees in computer science and engineering from Bangladesh University of Engineering and Technology in 2011 and 2009, respectively. He is a recipient of Ontario Graduate Scholarship, President's Graduate Scholarship, and David R. Cheriton Graduate Scholarship. He is a co-recipient of the Best Paper Award in the IEEE/ACM/IFIP CNSM 2019 and the IEEE/ACM/IFIP CNSM 2017 and the Best Student Paper Award in the IEEE NetSoft 2019. His research interests include network virtualization, 5G network slicing, and network reliability.

This article has been accepted for publication in a future issue of this journal, but has not been fully edited. Content may change prior to final publication. Citation information: DOI 10.1109/TNSM.2020.2992442, IEEE Transactions on Network and Service Management

Sepehr Taeb is a research assistant at the David R. Cheriton School of Computer Science, University of Waterloo. He received his B.Sc. in computer engineering from Sharif University of Technology in 2016, and the M.Math. degree in computer science from the University of Waterloo in 2019. His research interest includes network virtualization, optical networks, and Internet of drones.

Shihabur Rahman Chowdhury (S'13) is a PhD candidate at the David R. Cheriton School of Computer Science, University of Waterloo. He received his B.Sc. degree in computer science and engineering from BUET in 2009. His research interests include virtualization and softwarization of computer networks. He is co-recipient of the Best Paper Award at the IEEE/ACM/IFIP CNSM 2019, IEEE NetSoft 2019, and the IEEE/ACM/IFIP CNSM 2017 conference.

Mubeen Zulfiqar is pursuing his doctoral degree at the David R. Cheriton School of Computer Science, University of Waterloo. His research interest include network virtualization and network security.

Massimo Tornatore (SM) received the Ph.D. degree from Politecnico di Milano in 2006, where he is currently an Associate Professor with the Department of Electronics, Information, and Bioengineering. He also holds an appointment as an Adjunct Professor with the University of California at Davis, Davis, USA, and as a Visiting Professor with the University of Waterloo, Canada. His research interests include performance evaluation, optimization and design of communication networks (with an emphasis on the application of optical networking technologies), cloud computing, and machine learning application for network management. He has coauthored more than 300 peer-reviewed conference and journal papers (with 17 Best Paper Awards), 2 books and 1 patent, in the above areas. He is an Active Member of the Technical Program Committee of various networking conferences, such as INFOCOM, OFC, ICC, and GLOBECOM. He is a member of the Editorial Board of the IEEE Communication Surveys & Tutorials, IEEE Communication Letters, Photonic Network Communications (Springer), and Optical Switching and Networking (Elsevier).

Raouf Boutaba (F'12) received the M.Sc. and Ph.D. degrees in computer science from the University Pierre & Marie Curie, Paris, in 1990 and 1994, respectively. He is currently a professor of computer science and university research chair at the University of Waterloo. He is the founding editor in chief of the IEEE Transactions on Network and Service Management (2007–2010) and on the editorial boards of other journals. He received several best paper awards and recognitions including the Premier's Research Excellence Award, the IEEE ComSoc Hal Sobol, Fred W. Ellersick, Joe LociCero, Dan Stokesbury, Salah Aidarous Awards, and the IEEE Canada McNaughton Gold Medal. He is a fellow of the Royal Society of Canada, the Institute of Electrical and Electronics Engineers (IEEE), the Engineering Institute of Canada, and the Canadian Academy of Engineering. His research interests include resource and service management in networks and distributed systems.

Jeebak Mitra received the M.A.Sc. and Ph.D. degrees in electrical engineering from The University of British Columbia in 2005 and 2010, respectively. From 2010 to 2011, he was a Senior System Engineer with Riot Micro, leading the system level design for a local thermal equilibrium baseband. From 2011 to 2012, he was a Team Leader for physical layer DSP design with BLINQ Networks, Ottawa, focusing on small cell backhaul products. Since 2013, he has been a Senior Staff Engineer with the Huawei Technologies Canada Research Center, Ottawa, in the areas of algorithm design and implementation for coherent high-speed optical transceivers and flexible optical networks. His research interests lie in the area of high-performance communication systems design focusing on optical and wireless networks. He received the Best Student Paper Award at the IEEE Canadian Conference in Electrical and Computer Engineering 2009. He was a co-recipient of the Best Paper Award at IEEE/ACM/IFIP CNSM 2017 and 2019.

Mahdi Hemmati (M) is a Network Optimization Engineer at Huawei Technologies Canada Research Center. He received the PhD degree in Electrical and Computer Engineering from University of Ottawa in 2017. He received the NSERC Postgraduate Scholarship during his doctoral studies. Hemmati received his MSc in electrical engineering from Sharif University of Technology, Iran. His research interests include distributed control and optimization, fair resource allocation, and congestion control for multimedia applications. He was a co-recipient of the Best Paper Award at IEEE/ACM/IFIP CNSM 2019.